Examining the thermodynamic uncertainty relation for anomalous diffusion

Julius Johannes Taraz, 410064

1. Examiner	Prof. Dr. Sabine H. L. Klapp
2. Examiner	Prof. Dr. Holger Stark

1. Supervisor	Prof. Dr. Sabine H. L. Klapp
2. Supervisor	Dr. Seyed Mohsen Jebreiil Khadem

Technische Universität Berlin
Fakultät II - Mathematik und Naturwissenschaften
Institut für Theoretische Physik
Bachelor of Science

07.11.2022

Eidesstaatliche Erklärung

Hiermit erkläre ich, dass ich die vorliegende Arbeit selbstständig und eigenhändig sowie ohne unerlaubte fremde Hilfe und ausschließlich unter Verwendung der aufgeführten Quellen und Hilfsmittel angefertigt habe.

_____

Berlin, den 5. November 2022

Acknowledgments

First, I want to thank Prof. Dr. Sabine Klapp for the opportunity to write my Bachelor's thesis in her group. I want to thank her and Dr. Mohsen Khadem, my supervisors, for their directions, advice and help.
I especially want to thank Mohsen for his time, support and devotion to my questions and results, which I used extensively.
I am grateful to each and every member of the working group for the welcoming, inspiring and friendly atmosphere, insights, advice and the feeling of being part of the group. In particular, I thank Robin Kopp for reading a previous version of the thesis and providing many helpful comments.
Furthermore, I thank my friends and family for continuing to listen to my problems, for advice on English grammar, for reminding me of mathematical rigor and for ongoing support.
Special thanks go to my father and Katerina for a lot of time invested in this thesis.

Zusammenfassung

Die thermodynamische Unschärferelation (TUR) wird meist als untere Grenze für die Fluktuationen eines Stroms interpretiert. Diese untere Grenze kommt durch die Rate der Erzeugung von Entropie zustande. Die TUR kann allerdings auch als untere Grenze für den Diffusionskoeffizienten aufgefasst werden. Bei dieser Interpretation ist die Grenze durch die Mobilität der Teilchen gegeben. Es ist bekannt, dass die TUR für viele Systeme, wie überdämpfte Brownsche Molekularbewegung, molekulare Maschinen etc. gilt. Wir führen Langevindynamiksimulationen in zwei verschiedenen Modellen durch, um die Gültigkeit der TUR unter anomaler Diffusion zu untersuchen.
Einerseits betrachten wir ein überdämpftes Brownsches Teilchen in einem eindimensionalen Modell mit harmonischen Potentialen zufälliger Tiefe. Die Simulationsergebnisse werden mit analytischen Ausdrücken, wie den verallgemeinerten Lifson-Jackson Formeln, verglichen und die TUR wird untersucht. Wie durch die verallgemeinerten Lifson-Jackson Formeln hervorgesagt, verringern die Potentiale die Mobilität sehr. Die Verringerung der Mobilität ist stärker als die Verringerung des Diffusionskoeffizienten, sodass die TUR nicht verletzt wird.
Wir betrachten andererseits eine zweidimensionale exotische Umgebung, bestehend aus harten Hindernissen. Für über- und unterdämpfte Teilchen untersuchen wir den Einfluss von Hindernisdichte, Antriebskraft und anisotropem Rauschen auf Subdiffusion und die TUR. Die Mobilität wird durch eine Vergrößerung der Antriebskraft, eine Vergößerung der Hindernisdichte oder eine Verringerung des Rauschens senkrecht zur Antriebskraft verringert. Diese Verringerung führt für überdämpfte Teilchen wie im eindimensionalen Modell dazu, dass die TUR nicht verletzt wird. Wie erwartet gilt die TUR nicht für unterdämpfte Teilchen.

Abstract

The thermodynamic uncertainty relation (TUR) is usually interpreted as a lower bound on the fluctuations of a current. This lower bound is given by the entropy production rate. However, the TUR can also be interpreted as a lower bound on a particle's effective diffusion coefficient. In this case, the bound is given by the particle's mobility. It has been shown that the TUR applies for many systems including overdamped Brownian motion, molecular motors etc. We perform Brownian dynamics simulations in two different models to examine the validity of the TUR for anomalous diffusion.

On the one hand, an overdamped driven Brownian particle is considered in a one-dimensional model with random harmonic potentials. The results obtained with this simulation are compared to existing analytic expressions, such as the generalized Lifson-Jackson formula, and the TUR is reviewed. In agreement with the generalized Lifson-Jackson formulas, we find a strong decrease in the particle's mobility due to the square potentials. This decrease in mobility is stronger than the associated decrease in the effective diffusion coefficient, leading to a valid TUR.

On the other hand, simulations are done in a disordered medium in two dimensions with hard obstacles. We use over- and underdamped particles and review the influence of the obstacle density, the driving force and anisotropic noise on subdiffusion and the TUR. For overdamped particles we find similar results to the one-dimensional simulation. The strong decrease in mobility with an increasing driving force, an increasing obstacle density or a decreasing noise perpendicular to the driving force leads to a valid TUR for overdamped particles. As expected, the TUR does not remain valid for underdamped particles.

Table of Contents

1 Introduction

In this thesis, we examine the thermodynamic uncertainty relation (TUR) for anomalous diffusion.
Consider a molecule that is driven through a biological cell. Due to the non-zero temperature inside the cell, the molecule's position fluctuates. Which tools exist to quantify the fluctuations of the molecule's position?
On the one hand, macromolecules inside the cell must be accounted for [1]. This means the cell's interior is crowded, and the molecule moves only in the restricted space. In such a system, the diffusion of the molecule often is anomalous [2].
On the other hand, driving the molecule leads to non-equilibrium dynamics. Non-equilibrium states appear often, e.g., in active matter, such as biological systems [3]. For systems close to equilibrium, the fluctuations of stochastic trajectories can be quantified via the fluctuation-dissipation relation [4], which was proven in the 1950s [5]. But for systems far from equilibrium, only research of the last decade provided an inequality relating fluctuations and mean values of currents to the entropy production rate, the so-called TUR. It can also be interpreted as an upper bound on the "entropic cost" of a current's precision. The TUR is embedded in the framework of stochastic thermodynamics.
Stochastic thermodynamics is a research field that emerged in the last 30 years, in which principles of classical thermodynamics can be applied to stochastic systems [6–8]. Examples of stochastic trajectories in such systems are the position of a colloidal particle in a heat bath, the number of completed enzymatic cycles in a chemical reaction catalyzed by an enzyme or the position of an electron in a thermoelectric device. The TUR has been discovered for non-equilibrium Markovian systems [9, 10] and can be applied in many different ways. For example, it can be used to calculate the entropy production for short time scales [11] or to estimate the time span of anomalous diffusion in some systems [12]. Recently it was proven that non-Markovian systems violate the TUR [13, 14]. Some non-Markovian systems, such as those with fractional Brownian motion, generate anomalous diffusion. Thus the question arises whether the TUR remains valid for Markovian processes that exhibit (transient) anomalous diffusion. In this thesis, we address this question.
The thesis consists of an introductory chapter describing diffusion and the basics of stochastic thermodynamics. The chapter concludes with the analytic examination of the TUR for driven Brownian particles in free space.
In Chapter 2, a one-dimensional trap model for transient subdiffusion of driven and non-driven overdamped Brownian particles is described, and the numerical results obtained by simulations are discussed. Chapter 3 considers a two-dimensional disordered medium for driven and non-driven overdamped particles with isotropic and anisotropic noise. In Chapter 4, the same two-dimensional model with underdamped particles is reviewed.

1.1 Diffusion

1.1.1 Normal Diffusion

The first concept of relevance to this work is normal diffusion. A much more detailed introduction to the mathematical modeling of this phenomenon can be found in [15] among others.
In 1827 the botanist Robert Brown observed that grains of pollen perform "rapid oscillatory motion" in water [16]. In the early 1900s, Einstein [17] and Smoluchowski [18] investigated this phenomenon from the physical perspective. Parallelly Langevin put forward an alternative formulation of the problem [19]:
Consider a particle (colloid) with mass m suspended in a fluid along one axis. The colloid's dynamics can be described with Newton's second law

$$m\ddot{x} = -\gamma\dot{x} + F(x,t) + \eta(t), \tag{1.1}$$

where γ is the friction coefficient given by Stokes' law, F is an external force, and η is the fluctuating force. This type of equation is called a Langevin equation. The fluctuating force η results from the "kicks" of the surrounding fluid molecules. Since we assume that the fluid molecules move uncorrelated, the fluctuations at different times t_1 and t_2 have to be uncorrelated

$$\langle \eta(t_1)\eta(t_2)\rangle \sim \delta(t_1 - t_2), \tag{1.2}$$

and because of symmetry

$$\langle \eta(t)\rangle = 0, \tag{1.3}$$

where $\langle ...\rangle$ is the ensemble average over different noise realizations. The strength of the fluctuating force is given by the equipartition theorem

$$\eta(t) = \sqrt{2\gamma k_B T}\xi(t), \tag{1.4}$$

where $\xi(t)$ is a random variable with unit standard deviation, the Boltzmann constant is k_B, and T is the fluid's temperature. If an overdamped particle is considered

$$|m\ddot{x}| \ll |\gamma\dot{x}|, \tag{1.5}$$

the inertia term is negligible, and our Langevin equation reduces to

$$\gamma\dot{x} = F_c(x,t) + \sqrt{2\gamma k_B T}\xi(t). \tag{1.6}$$

By Fourier transforming the δ-correlation of the fluctuating force, we get a constant spectral power distribution and thus white noise. Since the central limit theorem applies to the random "kicks", the fluctuating force η has a Gaussian distribution [15].

For free diffusion, meaning no external force acting on the Brownian particle

$$\gamma\dot{x} = \sqrt{2\gamma k_B T}\xi(t), \tag{1.7}$$

various quantities are calculated, which are considered later to review the TUR. For the mean displacement relative to the initial position x_0, we get

$$\langle x(t) - x_0 \rangle = 0, \tag{1.8}$$

because the noise is symmetric. For the mean squared displacement (MSD, with respect to x), we calculate

$$\begin{aligned} MSD^{(x)}(t) &= \left\langle (x(t) - x_0)^2 \right\rangle = \left\langle \int_0^t \dot{x}(t_1)dt_1 \int_0^t \dot{x}(t_2)dt_2 \right\rangle \\ &= \left\langle \int_0^t \sqrt{2\frac{k_B T}{\gamma}}\xi(t_1)dt_1 \int_0^t \sqrt{2\frac{k_B T}{\gamma}}\xi(t_2)dt_2 \right\rangle \\ &= 2\frac{k_B T}{\gamma} \int_0^t \int_0^t \langle \xi(t_1)\xi(t_2) \rangle \, dt_1 dt_2 = 2\frac{k_B T}{\gamma} \int_0^t \int_0^t \delta(t_1 - t_2)dt_1 dt_2 \\ &= 2\frac{k_B T}{\gamma} \int_0^t dt_2 = 2\frac{k_B T}{\gamma} t =: 2Dt, \end{aligned} \tag{1.9}$$

where D is the diffusion coefficient. For the variance (with respect to x), we obtain

$$\begin{aligned} Var^{(x)}(t) &= \left\langle [(x(t) - x_0) - \langle x(t) - x_0 \rangle]^2 \right\rangle \\ &= \left\langle [x(t) - x_0]^2 - 2[x(t) - x_0]\langle x(t) - x_0 \rangle + \langle x(t) - x_0 \rangle^2 \right\rangle \\ &= MSD^{(x)}(t) - 2\langle x(t) - x_0 \rangle \langle x(t) - x_0 \rangle + \langle x(t) - x_0 \rangle^2 \\ &= MSD^{(x)}(t) - \langle x(t) - x_0 \rangle^2 = 2Dt. \end{aligned} \tag{1.10}$$

It follows that $Var^{(x)} = MSD^{(x)}$ if the mean displacement $\langle x - x_0 \rangle$ vanishes. From the overdamped Langevin equation, a Fokker-Planck equation [20, 21] can be derived

$$\dot{p}(x,t) = -\frac{\partial}{\partial x}\left(\frac{F(x,t)}{\gamma} p(x,t) \right) + D\frac{\partial^2}{\partial x^2} p(x,t), \tag{1.11}$$

which describes the time evolution of the probability density function p. In the case of free diffusion, $F = 0$, the Fokker-Planck equation is solved by

$$p(x,t) = \frac{1}{\sqrt{4\pi D t}} \exp\left(-\frac{(x - x_0)^2}{4Dt} \right) \tag{1.12}$$

for the initial distribution $p(x,0) = \delta(x - x_0)$. For example, this result can be obtained by a spatial Fourier transform of the Fokker-Planck equation. The ordinary differential equation in time regarding the Fourier transform can be solved by a Gaussian distribution, for $p(x,0) = \delta(x - x_0)$. The inverse transform thus yields a Gaussian distribution for p.

1.1.2 Anomalous Diffusion

As discussed in the previous section, the dynamics of a colloidal particle in a fluid can be described by normal diffusion. The central property of normal diffusion is the linear growth of the particle's variance in time. It is a well-understood process that has been studied for decades and can be derived from simple postulates [22]. Thus, it may be tempting or intuitive to apply this theory to many processes and view anomalous diffusion, which is characterized by a non-linearly growing variance, as a far-flung and unnatural phenomenon. The anomaly can be quantified as β the time-dependent exponent of anomalous diffusion

$$Var^{(x)}(t) \sim t^{\beta}. \tag{1.13}$$

For $\beta < 1$, the process is called subdiffusion, which is the focus of this work, and for $\beta > 1$, it is called superdiffusion. Converse to intuition, when studying natural phenomena anomalous diffusion is very common. Subdiffusion, for instance, occurs in crowded biological media [2], on cell membranes [23, 24] and in polymer chains [25] among many others. Subdiffusion is a general property of particle dynamics in inhomogeneous media [2]. It can be shown with various experimental techniques (e.g., fluorescence correlation spectroscopy or fluorescence recovery after photobleaching) that a multitude of (in vitro and in vivo) crowded biological media show subdiffusion [2, 26–28].
In addition, various mathematical models which model anomalous diffusion exist [2]. Some examples are trap models [29], continuous-time random walks (see Section 3.2.5) [30, 31], fractional Brownian motion [32, 33] and diffusion in disordered media [34, 35].
We want to focus on trap models and disordered media, mainly because with Gaussian white noise, there is a well-defined temperature, which is beneficial for stochastic thermodynamics. On the one hand, we consider particles in a one-dimensional random square potential in which the particles get trapped. This is described in more detail in Section 2.1. On the other hand, we consider a disordered medium in two dimensions. This means a Brownian particle diffuses around immobile obstacles; this is described in more depth in Section 3.1. Depending on the obstacle density ϱ, the diffusion will either be anomalous for transient times or for all times [36]. As we are proceeding to show, we examine whether the TUR can remain valid in case of long-term persisting subdiffusion.

1.2 Stochastic Thermodynamics

Classical thermodynamics (TD) describes the macroscopic behavior of large systems, being the average over a large ensemble, usually in equilibrium or using linear response theory close to equilibrium. On the other hand, stochastic TD describes the TD of mesoscopic systems such as single colloidal particles, for example, with the help of Langevin equations. Extensive reviews on stochastic TD can be found in [7, 8] among others.

1.2.1 Stochastic Energetics

Introduced by Sekimoto [6] in 1998, stochastic energetics is the framework in which energy accounting can be done for a single stochastic trajectory. The more recent formalism of thermodynamic quantities associated with single stochastic trajectory was introduced by Seifert in [37]. We now follow his calculations to introduce the entropy production for a single trajectory.

The dynamics of an overdamped Brownian particle with an external force $F(x,t)$, a friction coefficient γ, in a heat bath with temperature T and Gaussian white noise ξ with unit standard deviation can be described by a Langevin equation

$$\gamma\dot{x} = F(x,t) + \sqrt{2\gamma k_B T}\xi(t). \tag{1.14}$$

In the following, we choose units so that $k_B = 1$. The time evolution of the probability density function $p(x,t)$ can be described by the Fokker-Planck equation, see Equation (1.12). One can separate the force F into its conservative part and the non-conservative part

$$F = -\frac{\partial}{\partial x}U(x,\lambda) + f(x,\lambda(t)), \tag{1.15}$$

where $\lambda(t)$ is an external control protocol. The increment in work dW done on the system

$$dW = \frac{\partial U}{\partial \lambda}d\lambda + f dx \tag{1.16}$$

is the sum of the increment in potential due to the increment of protocol $d\lambda$ and the work done by the non-conservative force due to the particle's movement dx. The increment in potential dU

$$dU = \frac{\partial U}{\partial \lambda}d\lambda + \frac{\partial U}{\partial x}dx \tag{1.17}$$

is given by the differential of U. One then calculates

$$dW - dU = f dx - \frac{\partial U}{\partial x}dx = F dx =: dQ. \tag{1.18}$$

Where $dW - dU$ is identified with the increment in dissipated heat dQ. This is a formulation of the first law of thermodynamics for fluctuating trajectories. We can proceed to define the differential of the medium entropy production $dS_m = dQ/T$, which is a stochastic quantity. We introduce the action $A[x(\tau),\lambda(\tau)]$ of a trajectory $x(\tau)$ under the protocol $\lambda(\tau)$ to derive an equivalent expression for the entropy production ΔS_m. The path probability is given by

$$p[x(\tau),\lambda(\tau)] = N\exp(-A[x(\tau),\lambda(\tau)]). \tag{1.19}$$

The action is defined as

$$A[x(\tau),\lambda(\tau)] = \int_0^t \left[\frac{1}{4D}\left(\dot{x}(\tau) - \frac{F(x(\tau),\lambda(\tau))}{\gamma}\right)^2 + \frac{1}{2\gamma}\partial_x F(x(\tau),\lambda(\tau))\right]d\tau. \tag{1.20}$$

With a straightforward calculation we show

$$\dot{S}_m = F\dot{x}/T = -\dot{A}[x(\tau),\lambda(\tau)] + \dot{A}[x^\dagger(\tau),\lambda^\dagger(\tau)] = \frac{\dot{p}[x(\tau),\lambda(\tau)]}{p[x(\tau),\lambda(\tau)]} - \frac{\dot{p}[x^\dagger(\tau),\lambda^\dagger(\tau)]}{p[x^\dagger(\tau),\lambda^\dagger(\tau)]}. \tag{1.21}$$

Here, $x^\dagger(\tau) = x(t-\tau)$ is the reversed trajectory and $\lambda^\dagger(\tau) = \lambda(t-\tau)$ is the reversed protocol. $p[x^\dagger(\tau), \lambda^\dagger(\tau)]$ is the corresponding path probability. Thus, the medium entropy production along a trajectory is given by

$$\Delta S_m = \int_0^t \frac{dQ_\tau}{T} = \ln \frac{p[x(\tau), \lambda(\tau)]}{p[x^\dagger(\tau), \lambda^\dagger(\tau)]}. \tag{1.22}$$

One can then introduce the system entropy production of the trajectory, where $p(x,t)$ is a solution to the Fokker-Planck equation (1.12)

$$S_{sys}(t) = -\ln(p(x(t),t)). \tag{1.23}$$

The total entropy change can then be defined as

$$\Delta S_{tot} := \Delta S_m + \Delta S_{sys}. \tag{1.24}$$

It can be shown that ΔS_{tot} satisfies an integral fluctuation theorem

$$\langle e^{-\Delta S_{tot}} \rangle = 1 \Leftrightarrow \langle \Delta S_{tot} \rangle \geq 0. \tag{1.25}$$

This can be seen as an equivalent to the second law of thermodynamics for stochastic trajectories.

1.2.2 Fluctuation-dissipation relations

Fluctuation-dissipation relations (FDR) relate the dissipative properties of a system to its fluctuating properties for systems in equilibrium. For example, the friction coefficient γ quantifies a suspended particle's kinetic energy dissipation.
One prominent example of FDR is the relation between the diffusion coefficient (see Equation (1.9)) and the strength of the thermal noise (see Equation (1.4)). For a more detailed explanation, let us consider a free Brownian particle. This example is described in much more depth in [4]. From Equation (1.9) one can see that the following equation is an equivalent definition of the diffusion coefficient, if the mean displacement vanishes:

$$\begin{aligned} D &= \lim_{t\to\infty} \frac{1}{2t} \left\langle (x(t) - x_0)^2 \right\rangle = \lim_{t\to\infty} \frac{1}{2t} \int_0^t \int_0^t \langle \dot{x}(t_1)\dot{x}(t_2)\rangle dt_2 dt_1 \\ &= \lim_{t\to\infty} \frac{1}{t} \int_0^t \int_0^{t-t_1} \langle \dot{x}(t_1)\dot{x}(t_1+t')\rangle dt' dt_1 = \int_0^\infty \langle \dot{x}(t_0)\dot{x}(t_0+t)\rangle dt. \end{aligned} \tag{1.26}$$

Since white noise is δ-correlated, the integral converges. Now using Equation (1.9), we see

$$D = \frac{T}{\gamma} = \int_0^\infty dt \langle \dot{x}(t_0)\dot{x}(t_0+t)\rangle. \tag{1.27}$$

This relates the strength of the position's fluctuations $\dot{x}$, for a free Brownian particle, directly to the temperature T and to the dissipative quantity, which is the friction coefficient γ.

1.3 Thermodynamic Uncertainty Relation

In its most general form, the thermodynamic uncertainty relation (TUR) relates the precision of a current J to the entropy dissipated due to the generated current. The TUR was first discovered and derived for biomolecular processes [9]. Later it was shown that general continuous-time Markov processes [10] and overdamped Langevin systems arbitrarily far from equilibrium [38, 39] satisfy the TUR as well. The original version of the TUR (and the one used in this work) is valid in the steady state, meaning $J =$ constant. More recently, a TUR for transient times has been derived [39, 40].
There are various ways to derive the TUR. E.g., large deviation theory can be used [10, 41]. A relation between the variance, the mean and the large deviation function of the current and the mean entropy production is calculated, from which the inequality can be derived. The Cramér-Rao bound can also be used [40]. In this strategy, the information-theoretical quantities are identified with the thermodynamic quantities. A "direct" approach from the Langevin equation using only stochastic calculus also yields the TUR [42].
It has been shown that some systems violate the TUR. For example, it is violated for non-Markovian anomalous dynamics generated by fractional Brownian motion [13]. Since this work considers Markovian anomalous diffusion, this is a very relevant case of violation to us.
Other systems, such as underdamped systems [43], systems with a magnetic torque [44, 45] and the three-level maser [46], violate the (classical) TUR as well.
We will now derive the TUR for a very simple example, following [9]. Consider a jump process with position $x(t)$ at time t or equivalently a chemical reaction cycle, where $x(t)$ is the number of completed cycles at time t. The particle performs jumps, or the chemical reaction happens in one of the directions. Both actions $\Delta x = \pm 1$ have rates k^+ and k^- respectively. We consider the steady state, meaning the current $J = x(t)/t = k^+ - k^- =$ constant. We define the affinity A via the local detailed balance $k^+/k^- = \exp(A/T)$, where T is the temperature. We consider a waiting time distribution, e.g., a power-law waiting time distribution [31], that leads to the variance $Var^{(x)}(t) = (k^+ + k^-)t$.
Since the TUR only accounts for the entropy production rate σ associated with the affinity A, one has

$$\sigma = \frac{AJ}{T} = \frac{Ax}{Tt}. \tag{1.28}$$

We now define the uncertainty product

$$Q(t) := \frac{Var^{(x)}}{\langle x \rangle^2}\langle \sigma \rangle t = \frac{(k^+ + k^-)t}{(k^+ - k^-)^2 t^2}\frac{A}{T}(k^+ - k^-)t = \frac{k^+ + k^-}{k^+ - k^-}\frac{A}{T} = \frac{A}{T}\coth\left(\frac{A}{2T}\right). \tag{1.29}$$

$Q(A)$ attains its global minimum in equilibrium $Q(A = 0) = 2$, meaning

$$Q(t) = \frac{Var^{(x)}}{\langle x \rangle^2}\langle \sigma \rangle t \geq 2, \tag{1.30}$$

this is the TUR. Using the definition of the entropy production rate, the TUR is rewritten

$$Q(t) = \frac{A}{T}\frac{Var^{(x)}}{\langle x \rangle} \geq 2. \tag{1.31}$$

Since $\langle x \rangle \sim t$, the TUR would be violated for long times if $Var^{(x)} \sim t^{\beta}$ with $\beta < 1$. This motivates the investigation of the TUR for anomalous diffusion. As described in the introduction, the TUR can also be rearranged to [10]

$$\frac{Var(J)}{\langle J \rangle^2} \geq \frac{2}{\langle \sigma \rangle t}, \tag{1.32}$$

thus giving a bound for the current fluctuations. Finally, we rearrange the TUR to another equivalent version used later. We use the diffusion coefficient D, which we define similar to Equation (1.26),

$$D := \frac{Var^{(x)}}{2t} \tag{1.33}$$

and the average velocity v, which coincides with $\langle J \rangle$,

$$v := \frac{\langle x \rangle}{t} \tag{1.34}$$

to write

$$Q = \frac{A}{T}\frac{2Dt}{vt} = \frac{A}{T}\frac{2D}{v} \geq 2 \tag{1.35}$$

$$\Rightarrow D/T \geq v/A. \tag{1.36}$$

The affinity A will be replaced by the driving force f in the following.

1.3.1 Driven Brownian particle

In this section, we review the TUR for a driven Brownian particle analytically. For this we need to calculate $\langle x \rangle$ and $Var^{(x)}$. Consider an overdamped Brownian particle driven by a constant force f. Note that unlike in Section 1.2.1, the force denoted by f is conservative. In this case the affinity A is equal to f, the driving force [12]. In the following, we set $x_0 = 0$. The Langevin equation describing the dynamics thus reads

$$\gamma \dot{x} = f + \sqrt{2\gamma T}\xi(t). \tag{1.37}$$

We then obtain

$$\langle \dot{x} \rangle = \frac{f}{\gamma} \Rightarrow \langle x \rangle = \frac{f}{\gamma}t \tag{1.38}$$

$$\text{and } Var^{(x)} = MSD - \langle x \rangle^2 = \frac{2T}{\gamma}t \tag{1.39}$$

with which we can calculate the uncertainty product, (Equation (1.31)),

$$Q(t) = \frac{f}{T}\frac{2Tt/\gamma}{ft/\gamma} = 2. \tag{1.40}$$

This means that $Q(t)$ is minimal for a driven Brownian particle. Both sides of the TUR are equal.

1.4 Units

For notational convenience, we choose units so that $k_B = 1$ and $\gamma = 1$. Distances are measured in trap or obstacle radii R and times in Brownian times τ_B. This leads to the following units for the quantities used. Unless stated otherwise, the temperature $T = 1R^2/\tau_B$ is used in the simulations. For convenience, T is used as a unit as well.

Table 1.1: Units used in the following chapters.

Quantity	Distance x	Time t	Temp. T	Diff. coeff. D	Potential U	Force F	Velocity v	Mass m
Unit	R	τ_B	R^2/τ_B	$T = R^2/\tau_B$	$T = R^2/\tau_B$	R/τ_B	R/τ_B	τ_B

2 One-dimensional Model

In this chapter, a one-dimensional model in which Brownian particles are trapped in attractive potentials is described, then the numerical results for the diffusion coefficient and the average velocity obtained with this model are compared to the results of analytic expressions. Lastly, the TUR is reviewed in this model. As we are proceeding to show, the TUR is valid as an inequality for moderate driving forces due to giant diffusion. On the other hand, the TUR becomes a tight bound for very small and high driving forces.

2.1 Model

We construct a one-dimensional trap model in which Brownian particles move through a potential landscape with attractive potentials. For the force at position x, we choose

$$F(x) = -\sum_j \hat{U}_j \frac{x - 2Rj}{R} \Theta(R - |x - 2Rj|), \tag{2.1}$$

where the Heaviside step function is

$$\Theta(x) = \begin{cases} 1 & \text{for } x > 0 \\ 0 & \text{for } x \leq 0. \end{cases} \tag{2.2}$$

This means the traps are modeled as harmonic potentials, which are cut off at a distance R and are periodically located at $2Rj$ with the trap index j.
The traps each have a strength $\hat{U}_j > 0$. The strength is a random variable distributed uniformly in the interval $(0, \hat{U}_{max})$.
The Langevin equation describes the dynamics of the particle in our one-dimensional model

$$\dot{x} = f + F(x) + \sqrt{2T}\zeta(t), \tag{2.3}$$

where $F(x)$ is the trapping force, and f is the constant driving force. The other variables used here were introduced in Section 1. As described in Section 1.4 we chose units in a way that leads to $\gamma = 1$ and $k_B = 1$. We find

$$U(x) = \sum_j \hat{U}_j \frac{(x - 2Rj)^2 - R^2}{2R} \Theta(R - |x - 2Rj|) \tag{2.4}$$

to be a continuous potential with $F = -\frac{\partial U}{\partial x}$.
A possible potential landscape is shown in Figure 2.1. Unless stated otherwise, the simulations are computed with $T = 1R^2/\tau_B$. The Euler-Maruyama integration scheme [47] is used. Therefore the variance of the numerical values of the noise is not given by $\sqrt{2T}$ but by $\sqrt{2T/\Delta t}$ where Δt is the numerical time step [48]. The calculations are done for multiple realizations of the noise and multiple realizations of the landscape; a quenched average is done. The results of the simulations represent the steady state.

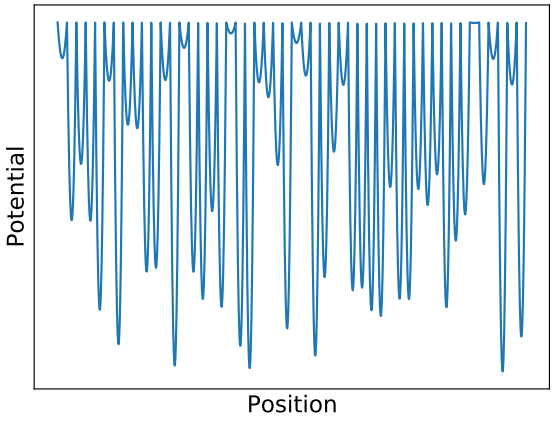

Figure 2.1: Possible potential landscape used in the one-dimensional model. The potential consists of individual harmonic potentials (traps). The traps are placed directly next to each other. Each trap has a finite range R. The traps have random strengths, which are uniformly distributed in an interval $(0, \hat{U}_{max})$.

The diffusion coefficient D and the effective velocity v are calculated via curve fitting from the numerical data. They are fit parameters in the logarithmized Equations (1.33) and (1.34) respectively. D is the diffusion coefficient for long times. For small times, the relative fluctuations in $\langle x \rangle$ are large. Therefore, the curve fit is only calculated with the data points with times $t \in (10^n \Delta t, 10^{n+1} \Delta t)$, where Δt is again the numerical time step, and n is given by the trajectory's length. In the one-dimensional case the superscript (x) for Var is omitted.
The Levenberg-Marquardt-algorithm is used for the curve fitting [49]. The measurement uncertainty Δ_j of the j-th fit parameter can be calculated as

$$\Delta_j = \sqrt{C_{jj}}, \tag{2.5}$$

where C is the covariance matrix.

2.2 Analytic expressions

In 1962 Lifson and Jackson [50] considered an ion diffusing with a potential $U(x)$ generated by two charged plates at $x = 0$ and $x = L$. The particle's dynamics is described by the Langevin equation

$$\dot{x} = -\frac{\partial}{\partial x} U(x) + \sqrt{2T}\xi(t). \tag{2.6}$$

Lifson and Jackson calculated the average time τ for the ion to arrive at one of the plates from the initial position $x_0 = L/2$ to be

$$\tau = \frac{1}{D_0} \int_{L/2}^{L} dx' \exp\big(-U(x')/T\big) \int_{L/2}^{x'} dx'' \exp\big(U(x'')/T\big), \tag{2.7}$$

where $D_0 = T$ is the free diffusion coefficient.

By defining the effective diffusion coefficient as $D_{LJ} := \frac{L^2}{2\tau}$ and defining

$$\langle \exp(\pm U/T) \rangle := \frac{1}{L} \int_0^L dx \exp(\pm U(x)/T), \tag{2.8}$$

they then showed that

$$D_{LJ} = \frac{D_0}{\langle \exp(+U/T) \rangle \langle \exp(-U/T) \rangle}. \tag{2.9}$$

Now we turn to a tilted washboard potential with a driving force f and the potential $U(x)$, such as our model,

$$\dot{x} = f - \frac{\partial}{\partial x} U(x) + \sqrt{2T}\xi(t). \tag{2.10}$$

In 2001, Reimann et al. [51] showed that the mean velocity is

$$v_{gLJ} := \frac{\langle x \rangle}{t} = D_0 L \frac{1 - \exp(-Lf/T)}{\int_0^L dx I_+(x)} \tag{2.11}$$

and that the effective diffusion coefficient is

$$D_{gLJ} := \frac{L^2}{2\tau} = D_0 L^2 \frac{\int_0^L dx I_+^2(x) I_-(x)}{\left(\int_0^L dx I_+(x) \right)^3}, \tag{2.12}$$

$$\text{where } I_\pm(x) := \int_0^L dx' \exp\big([\pm U(x) \mp U(x \mp x') - x'f]/T \big). \tag{2.13}$$

In 2019 Berezhkovskii and Dagdug [52] proved Equation (2.12) to be equivalent to

$$D_{gLJ} = \frac{D_0}{\langle \exp(+[U - fx]/T) \rangle \langle \exp(-[U - fx]/T) \rangle} \left(\frac{\sinh(fL/(2T))}{fL/(2T)} \right)^2. \tag{2.14}$$

Here, $U(x) - fx$ is a non-periodic potential. It can easily be shown that for $f = 0$ this is equivalent to Equation (2.9). Thus the equation is called the generalized Lifson-Jackson formula. For the comparison to the numerical data, the integrals are evaluated numerically with the simple rectangle rule. The interval $(0, L)$ is discretized by 10^4 points.

2.3 Results

2.3.1 Subdiffusion of non-driven particles

First, we review the variance of the position for non-driven particles $f = 0$. For different $\hat{U}_{max}$, we see the variance over time in Figure 2.2. We note that we do not see subdiffusion at long times.

For a large $\hat{U}_{max}$, the particles are trapped at $Var/R^2 \approx 0.1 < (1/2)^2 = 0.25$. We compare the variance to $(R/2)^2$ because if the particles were initially distributed uniformly over a trap, $R/2$ would be the average distance to the potential minimum. In a steady state the particles are already trapped around the potential minimum in the beginning. Thus, $R/2$ is the upper bound on the distance.

Since $\hat{U}_{max}$ is finite, so is the average time the particles are trapped in the potential. This leads to normal diffusion for long times. Thus, the effective diffusion coefficient $D(\hat{U}_{max})$ is constant for long times, see Equation (1.33).

We now compare our results for the effective diffusion coefficient $D(\hat{U}_{max})$ with the analytic predictions. As described in Section 2.2, Lifson and Jackson (LJ) derived an analytic expression for the effective diffusion coefficient D_{LJ} for various periodic potentials [50].

As stated in Section 2.1, the potential used in the simulation is described by Equation (2.4), where the individual traps have a random strength, distributed uniformly in the interval $(0, \hat{U}_{max})$. In the following, the same potential is used for the analytic prediction but with the difference that $\hat{U}_j = \hat{U} =$ constant for all j. The diffusion coefficient calculated analytically is $D_{LJ}(\hat{U})$. The formula used for the analytic prediction and its evaluation is described in Section 2.2. The comparison is shown in Figure 2.3. The data is compared to $D_{LJ}(\hat{U} = \hat{U}_{max})$, $D_{LJ}(\hat{U} = \hat{U}_{max}/2)$ (thus the average potential strength) and a value between both $D_{LJ}(\hat{U} = 0.85\hat{U}_{max})$. The prediction of $\hat{U} = 0.85\hat{U}_{max}$ agrees very well with the simulated data. This means that deeper potentials have a stronger effect than the weaker traps.

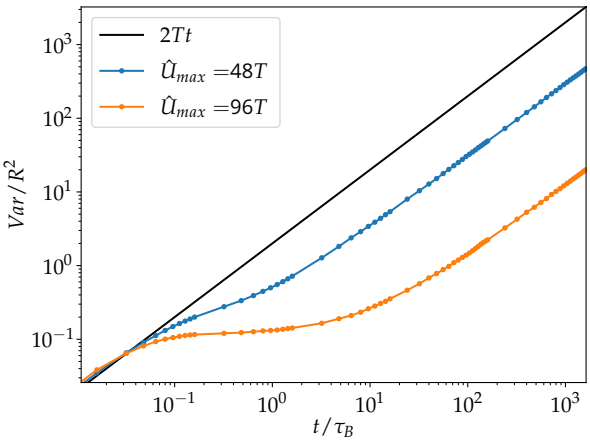

Figure 2.2: Variance of the position over time for different $\hat{U}_{max}$ for the non-driven particle in the trap model in comparison with the variance for free diffusion $Var(t) = 2Tt$.

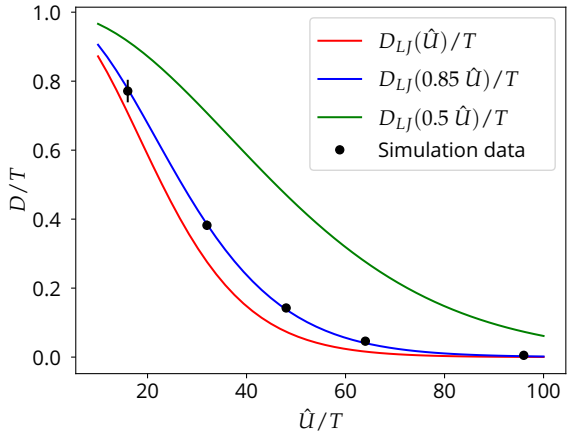

Figure 2.3: D/T versus $\hat{U}$. The simulation data (black) for the trap model is compared to the predictions of the LJ formula (see Section 2.2) for different $\hat{U}$. The comparison is done with D_{LJ} for $\hat{U} = \hat{U}_{max}$ (red), the average potential strength $\hat{U} = 0.5\hat{U}_{max}$ (green) and a potential strength in between (blue). The diffusion coefficient D is calculated as the fit parameter in the equation $\ln(Var(t)) = \ln(2Dt)$. The curve fit is applied to the data with time $t \in (10^2\tau_b, 10^3\tau_B)$. The error bars are calculated via Equation (2.5).

2.3.2 Giant diffusion

After discussing the variance of the position for non-driven particles, we now turn to driven particles. We briefly discuss existing work on tilted washboard potentials and compare our results to the existing work for the mean position and the variance or equivalently for the effective velocity and the diffusion coefficient. A Brownian particle in a tilted washboard potential can be described by the Langevin Equation

$$\dot{x} = f - 2\pi\frac{\hat{U}}{L}\sin(2\pi x/L) + \sqrt{2T}\xi(t). \tag{2.15}$$

The system is characterized by the tilt f (which is the driving force) and the strength of the traps $\hat{U}$. The particle can have a long-time effective diffusion coefficient $D(f,\hat{U})$ that is greater than the diffusion coefficient for free diffusion $D_0 = k_B T/\gamma = T$ (in our system of constants). This effect is called giant or enhanced diffusion [51] and has also been studied experimentally [53].
The effect can be explained as follows. The size of each trap is $L = 2R$ and thus the periodicity of the potential is given by $U(x) = U(x+L)$. If $\hat{U}/L \gg f$, the particle is trapped, implying $D(f,\hat{U}) < D_0$. If $f \gg \hat{U}/L$, the potential is negligible compared to the driving force and the particle diffuses freely, meaning $D(f,\hat{U}) \to D_0$. If $\hat{U}/L \approx f$, the external force acting on the particle varies strongly with its position. The position oscillates strongly around the mean position, thus $D(f,\hat{U}) > D_0$.
For a trigonometric potential, the diffusion coefficient $D(f)$ attains its maximum at $f = \hat{U}/L$. The potential described in Equation (2.4) yields a similar phenomenon.

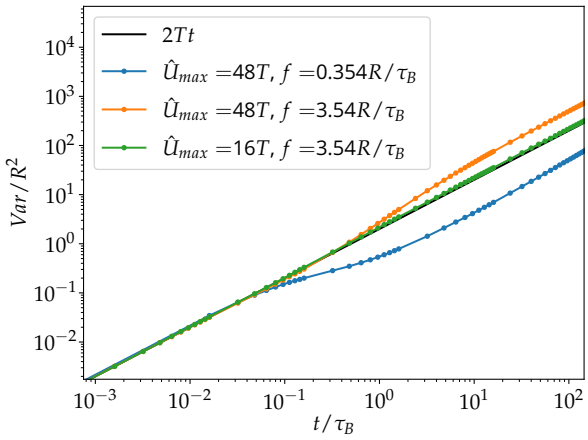

Figure 2.4: Variance of the position over time for various values of $\hat{U}_{max}$ and f for the driven particle in the trap model in comparison with $Var^{(x)}(t) = 2Tt$ for free diffusion.

A few exemplary curves for $Var(t)$ can be seen in Figure 2.4. For small f compared to $\hat{U}_{max}$ (blue), the diffusion coefficient D is lower than T, which is the diffusion coefficient for free diffusion. For moderate f (orange), we observe $D > T$ and thus enhanced diffusion. For large f (green), D will approach T from above. The variance for free diffusion $2Tt$ can be seen very close to the green line in black.
In the steady state we observe the mean position of the particle $\langle x\rangle$ to grow linear in time (as seen in Figure 2.5). We then define the average velocity as $v = \langle x\rangle/t$, which decreases with increasing $\hat{U}_{max}$ and increases with increasing f. By comparing v for a given f and $\hat{U}_{max}$ it can be seen that $v < f$ for all values of f and $\hat{U}_{max}$.
Building on the work of Lifson and Jackson, many analytic expressions for the diffusion coefficient $D_{gLJ}(f \neq 0, \hat{U})$ for tilted arbitrary periodic potentials, so-called generalized Lifson-Jackson (gLJ) formulas, have been derived [51, 52, 54–56]. Also a formula for the average velocity in the steady state $v_{gLJ}(f,\hat{U})$ has been derived [51]. The used formulas are listed and their evaluation is described in Section 2.2.

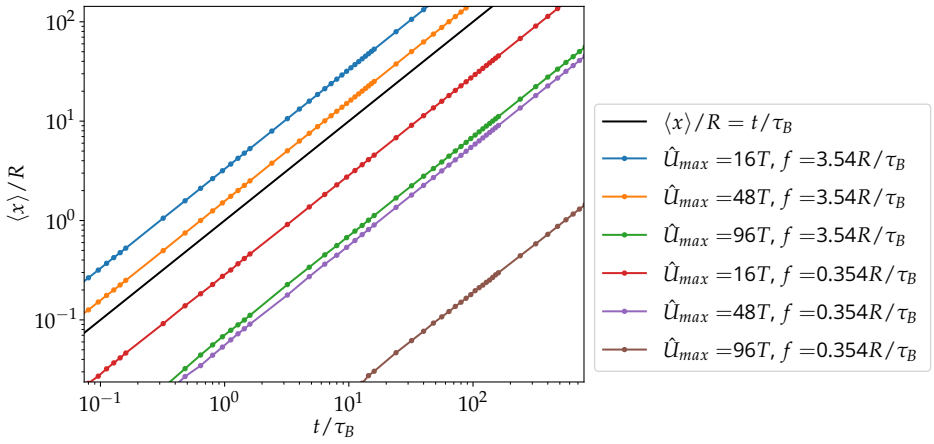

Figure 2.5: Mean position of the driven particle in the trap model over time for potential strengths $\hat{U}_{max}/T \in \{16, 48, 96\}$ and driving forces $f/(R/\tau_B) \in \{0.354, 3.54\}$. For comparison, the theoretical mean position of a particle driven with $f = 1R/\tau_B$ and $\hat{U}_{max} = 0$ is shown in black. This particle would have the mean position $\langle x\rangle/R = t/\tau_B$.

We now compare the simulated data for different f and $\hat{U}_{max} =$ const. with the analytic predictions.
Very similar to Section 2.3.1 the potential for the analytic predictions is given in Equation (2.4) with $\hat{U}_j = \hat{U} =$ const. for all j. The individual traps in the simulation have random strengths, distributed uniformly in the interval $(0, \hat{U}_{max})$.
The comparison can be seen in Figure 2.6. Again similar to the previous section, the simulated data is compared to the maximum strength $\hat{U} = \hat{U}_{max} = 16T$, the average potential strength $\hat{U} = \hat{U}_{max}/2 = 8T$ and a value between those $\hat{U} = 10.25T$.
The agreement between the prediction (for $\hat{U} = 10.25T$) and the data is especially found for large values of f. For small to moderate f, there is a qualitative agreement for the dependency of f. For moderate to large f, the agreement for v/f is good. The deviations for small f are bigger because for small f, the particles are most likely trapped in the deepest potentials. Since the deepest potentials have a strength $\hat{U} = \hat{U}_{max}$, the red curves give a lower bound for the simulation data for small f.
The evaluation of the gLJ formulas, Section 2.2, shows that in the small f regime, we find that

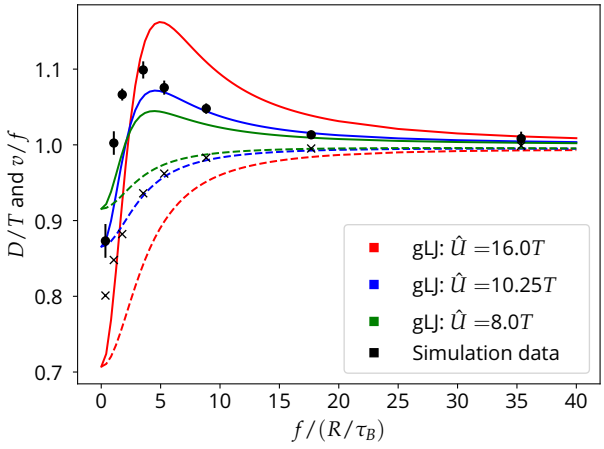

Figure 2.6: D/T and v/f versus f. The simulation data (black) for the trap model is compared to the predictions of the gLJ formulas for different $\hat{U}$. The average (green), the maximum (red) and a potential strength in between (blue) are represented. For D/T, the simulation data is shown as dots and the gLJ predictions are shown as solid lines. For v/f, the simulation data is shown as crosses and the gLJ predictions are shown as dashed lines. The effective diffusion coefficient D and the mean velocity v are calculated from the simulation data as fit parameters in the equations $\ln(Var(t)) = \ln(2Dt)$ and $\ln(\langle x\rangle(t)) = vt$ respectively. The curve fit is applied to the data with time $t \in (10^2\tau_b, 10^3\tau_B)$. The error bars are calculated via Equation (2.5).

$D_{gLJ}/T > v_{gLJ}/f$ as well, see Figure 2.7. The meaning of this comparison will be explained in the next section. As $f \to 0$, we see that D/T and v/f approach each other closely for each potential strength $\hat{U}$.

2.3.3 Uncertainty product affected by the driving force

In the previous section, we examined analytic expressions and our numerical results for the mean position and the variance of the position. Now we review the TUR with the help of those previously discussed results. For this review, we use Equations (1.31) and (1.36).
In Section 2.3.2 we saw that $v/f < 1$ for all values of f and $\hat{U}_{max}$. We also observed that the diffusion coefficient for small times $D(t \to 0) = D_0 = T$ (see Figure 2.4). For large f we know that $D \to D_0 = T$ (from above) and $v/f \to 1$ (from below), implying that the TUR becomes tight. In the limit of $f \to \infty$, this is free diffusion (Section 1.3.1). For giant diffusion we find $D(t \to \infty) > D(t \to 0) = T$ and thus the time-dependent diffusion coefficient D increases over time. This means the uncertainty product $Q(t) \sim D(t)/v$ (Equation (1.35)) increases over time as well, see Figure 2.8 (orange). Since $v/f < 1 = D(t \to 0)/T$, the TUR is not violated for small times, see Equation (1.36), and thus never.

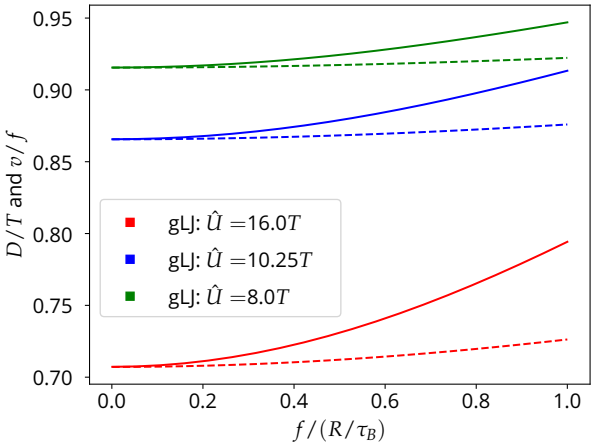

Figure 2.7: D/T (solid lines) and mobility v/f (dashed lines) for Brownian particles in a tilted washboard potential calculated with the gLJ formulas, Section 2.2, for three different potential strengths $\hat{U}$.

For negligible giant diffusion (small f) the diffusion coefficient $D(t)$ decreases over time. Figure 2.8 (blue) shows the uncertainty product $Q(t)$ for such a case.
In Figure 2.9 we compare D/T and v/f for very small values of f. It has to be noted that, since $f/(R/\tau_B) \leq 0.02$ is much smaller than the noise intensity $\sqrt{2T} \approx 1.4$, the results are very noisy. This manifests itself in the significant measurement uncertainties (shown as error bars). From this data a violation in the small f limit for $\hat{U}_{max} = 96T$ can not be anticipated. From the gLJ formulas we know that $D/T > v/f$ for small f as well, see Figure 2.7.
To show all regimes of f we show how the minimal uncertainty product $Q_{min} = \min_t Q(t)$ depends on f for a constant $\hat{U}_{max}$ in Figure 2.10 . As we can see Q_{min} has a non-monotonic dependency on f. In agreement with our calculations for free diffusion (see Section 1.3.1) we find that $\lim_{f\to\infty} Q_{min} = 2$. We find a maximum of Q_{min} at a finite non-zero f.
In the following, we describe how the measurement uncertainty Δ (represented as an error bar) of Q_{min} is obtained. Let $Q(t)$ attain its minimum at $t = \tau_i$ and let the simulation have data saved for $t = \tau_j, j \in (0, N)$, then $\Delta = \sum_{k=i-2}^{i+2} Q(\tau_k)/5 - Q(\tau_i)$.
Finally we can write the TUR as $\frac{Var^{(x)}}{\langle x \rangle^2} t \geq \frac{2}{\langle \sigma \rangle}$ (see Equation (1.30)), where $\sigma = \frac{f}{T}\frac{x}{t}$ is the medium entropy production rate (see Equation (1.28)). Figure 2.11 shows $min_t \left(Var^{(x)}(t) \cdot t / \langle x(t) \rangle^2 \right)$ versus $\langle \sigma \rangle$. The figure shows that the lower bound is closely approached for very small and large $\langle \sigma \rangle$. For small $\langle \sigma \rangle$ (implying small f and thus systems close to equilibrium), we saw the close bound of D/T and v/f in Figures 2.7 and 2.9. On the other hand, large values of σ are achieved by high f and low $\hat{U}_{max}$, thus approaching free diffusion.

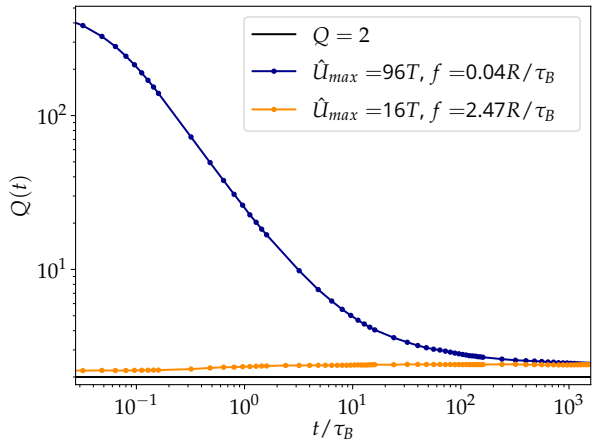

Figure 2.8: Uncertainty product $Q(t)$ over time for the driven particle in the trap model for the maximum potential strength $\hat{U}_{max} = 96T$ and the driving force $f = 0.04R/\tau_B$ (blue) and $\hat{U}_{max} = 16T, f = 2.47R/\tau_B$ (orange). For comparison, the lower bound on the uncertainty product $Q = 2$ given by the TUR is shown in black. Note both axes are scaled logarithmically.

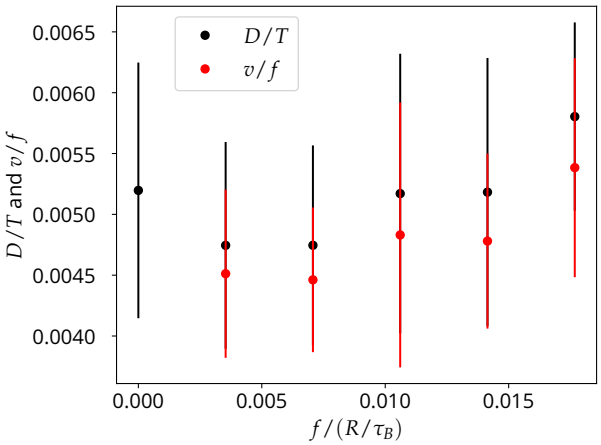

Figure 2.9: Numerical results D/T and v/f versus f for a fixed $\hat{U}_{max} = 96T$ for small f for the driven particle in the trap model. Using the equations $\ln(Var(t)) = \ln(2Dt)$ and $\ln(\langle x \rangle(t)) = vt$ we calculate D and v as fit parameters. The curve fit is applied to the data with time $t \in (10^2\tau_b, 10^3\tau_B)$. The error bars are calculated via Equation (2.5).

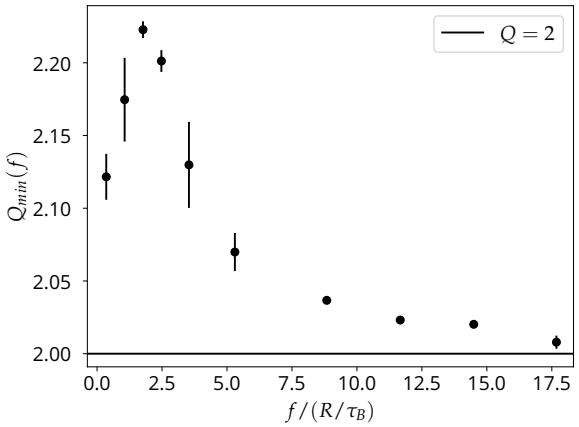

Figure 2.10: The minimal uncertainty product Q_{min} versus the driving force f with the maximum potential strength $\hat{U}_{max} = 16T$ for driven particles in the trap model. The measurement uncertainties are given by the deviation of the minimal value from the average of its five surrounding values. For comparison, the lower bound on the uncertainty product $Q = 2$ given by the TUR is shown in black.

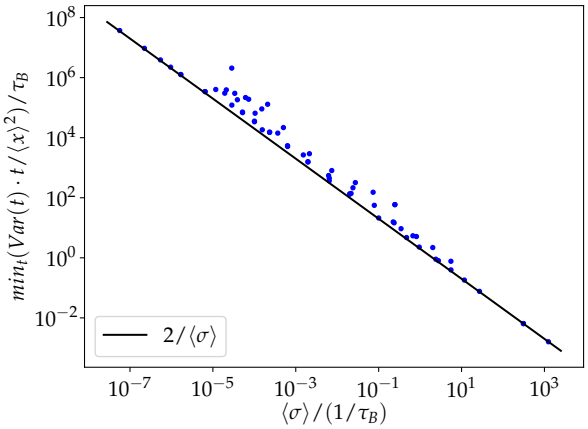

Figure 2.11: This figure shows $min_t\left(\frac{Var^{\langle x\rangle(t)}}{\langle x(t)\rangle^2}t\right)$ for multiple parameter settings versus the average medium entropy production rate $\langle\sigma\rangle$ in comparison to the lower bound $2/\langle\sigma\rangle$ given by the TUR for the driven particle in the trap model. The units used refer to the usually used trap radius $R = 0.25$ and $T = 1$. The trap radii used are $R, 2R$ and $4R$. The temperatures used are $0.1T, 0.5T, T, 2T$ and $5T$. The trap strengths are $\hat{U}_{max}/T \in \{16, 32, 48, 64, 80, 96, 112, 128, 154\}$. The values for the driving force all lay in the interval $f/(R/\tau_B) \in (0.003525, 35.25)$. The parameters are not chosen randomly from those intervals.

3 Two-dimensional Model

In this chapter, a two-dimensional model in which Brownian particles move in a disordered medium is described. The numerical results for the variance of the position of non-driven particles are compared to the literature regarding the percolation transition. Finally, the variance of the position, the mean position and the uncertainty product of driven particles are calculated. The influence of different densities, different driving forces and anisotropic noise is investigated. As we demonstrate in this chapter, the TUR only provides a tight bound for low obstacle densities, small driving forces or strong noise perpendicular to the driving force. As the system parameters change opposite to the aforementioned directions, the TUR becomes an increasingly loose bound. The TUR remains anyways valid.

3.1 Model

As described in Section 1.1.2, a (tracer) particle moving in a disordered medium (see Figure 3.1) exhibits subdiffusion.
The dynamics of a driven particle is described with the Langevin equation

$$\dot{\vec{r}} = f\vec{e}_x + \sqrt{2T}\vec{\xi}(t). \tag{3.1}$$

As described in Section 1.4, we choose $k_B = \gamma = 1$. The Langevin equation does not include the obstacles yet. The simulation is done in a square with side length $L = 891R$ and periodic boundary conditions. To model the particle's interaction with the solid obstacles, we use the Cichocki-Hinsen algorithm [57] with the Euler-Maruyama integration scheme [47] and the numerical time step Δt. The algorithm states the following for each iteration.

- In iteration i the particle has position $\vec{r}_i$.
- From Equation (3.1) it follows $\Delta\vec{r} = \Delta t(f\vec{e}_x + \sqrt{2T}\vec{\xi}(t))$.
- Is the proposed new position $\vec{r}_i + \Delta\vec{r}$ inside a solid obstacle?
  1. If yes, the particle stays in its position $\vec{r}_{i+1} = \vec{r}_i$.
  2. If no, the particle moves accordingly $\vec{r}_{i+1} = \vec{r}_i + \Delta r$.

Similar algorithms are used in e.g., [57–59].
We use N randomly placed circular obstacles with radius R. This implies the possibility of overlapping. Thus, the obstacle density ϱ, or the covered area fraction, is on average not $N\frac{\pi R^2}{L^2}$.

In Section 3.3, we prove that the mean effectively covered area fraction is

$$\varrho = 1 - \left(1 - \frac{\pi R^2}{L^2}\right)^N. \tag{3.2}$$

This is the average over all the obstacle configurations.
To accelerate the computation, a grid was used. This means, the whole area was divided into squares (grid cells) of side length $4R$. For each grid cell, the indices of the obstacles whose centers were located in this cell were noted in a list. If the particle is located in the (i, j) cell, the Cichocki-Hinsen algorithm only had to be applied to the obstacles placed in this cell and the adjacent cells $(i + k, j + l)$ for all $k, l \in \{-1, 0, 1\}$. For boundary cells, this has to be adjusted. This use of the grid is based on the assumption that the particle does not move further than $4R$ in one iteration.

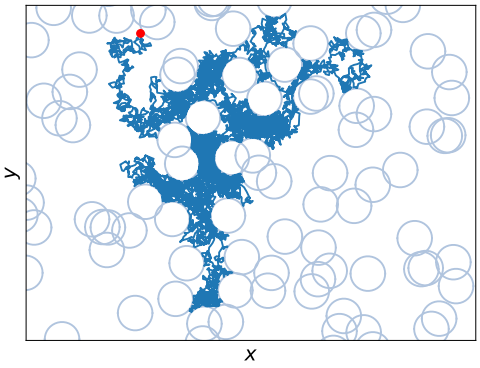

Figure 3.1: This figure shows an example trajectory of a diffusing Brownian particle in a two-dimensional disordered medium. The disordered medium consists of overlapping circular obstacles of uniform size. The particle's movement started at the red dot.

The results of the simulations only represent the steady state. The exponent of anomalous diffusion β and the mean velocity v are calculated via curve fitting from the numerical data. They are fit parameters in the logarithmized Equations (1.13) and (1.34) respectively. The exponent of anomalous diffusion for intermediate times is β_{im}, the curve fit is calculated with the data points with times $t \in (20\tau_B, 300\tau_B)$, where Δt is the numerical time step. Since the relative fluctuations in $\langle x \rangle$ are significant for small times, the curve fit is only calculated with the data points with times $t \in (10^4\tau_B, 10^5\tau_B)$ unless stated otherwise.

3.1.1 Model for the supplementary simulations

We again consider a tracer particle in a disordered medium. The obstacles in this simulation are soft, meaning the interaction of the tracer with the obstacles can be described with the Langevin equation

$$\dot{\vec{r}} = f\vec{e}_x - \sum_j \vec{\nabla} U(|\vec{r} - \vec{x}_j|) + \sqrt{2T}\vec{\xi}(t). \tag{3.3}$$

We model the soft obstacles with a purely repulsive Lennard-Jones potential (Weeks-Chandler-Andersen potential)

$$U(r) = \begin{cases} U_0 \left(\frac{1}{4(r/R)^{12}} - \frac{1}{2(r/R)^6} + \frac{1}{4} \right) & \text{for } r < R \\ 0 & \text{for } r \geq R, \end{cases} \tag{3.4}$$

where R is the radius of the obstacle, U_0 is the obstacle's potential strength and $\vec{x}_j$ is the position of the j-th obstacle. The radius and the strength of the potential are constant for each obstacle. The density is calculated with the same formula as for the other two-dimensional model, see Equation (3.2). In this section, we employ time averages to calculate the defined quantities. Namely, the time-averaged mean squared displacement MSD_{TA}, the time-averaged mean dis-

placement $\langle x \rangle_{TA}$ and the time-averaged variance are calculated via

$$MSD^{(x)}_{TA}(t) = \frac{1}{T-t}\int_t^T (x(\tau) - x(\tau - t))^2 d\tau, \tag{3.5}$$

$$\langle x \rangle_{TA}(t) = \frac{1}{T-t}\int_t^T (x(\tau) - x(\tau - t)) d\tau, \tag{3.6}$$

$$Var^{(x)}_{TA}(t) = MSD^{(x)}_{TA}(t) - \langle x \rangle^2_{TA}(t). \tag{3.7}$$

For ergodic systems and infinite observation time, the time-averaged quantities are equal to the corresponding ensemble-averaged quantities [59]. The results, obtained from the model described in this section, qualitatively agree with those obtained from the model of the previous section.

3.2 Results

3.2.1 Subdiffusion of a non-driven particle

First, we review the variance of the position for non-driven particles for different obstacle densities. The variance and the exponent of anomalous diffusion for intermediate times are shown in Figure 3.2. One sees that for all densities at small times, the variance behaves similarly to the variance of a particle in free space $Var^{(x)} = 2Tt$. Initially, the particles move in free space until they collide with the obstacles. The obstacle interactions lead to the deviation from the free diffusion behavior at around $Var^{(x)} \approx R^2$. At this point, the particles have covered a distance of R on average, which is also the average distance between the obstacles for the densities shown [35, 60]. The effective diffusion coefficient is reduced by the obstacle interaction. Thus, one observes subdiffusion for all densities for intermediate times. This can be seen in the exponent of anomalous diffusion β_{im}. For low densities, the diffusion is normal for long time scales. For densities above the critical density for percolation $\varrho_c = 0.67$, the variance does not grow linear for long times and the diffusion remains anomalous. For even higher densities the variance saturates. The critical density and the corresponding exponent of anomalous diffusion $\beta(\varrho_c) \approx 0.66$ agree with the literature such as [35, 61] (note that a conversion of quantities has to be done). Long-time subdiffusion happens if the obstacles form a percolating cluster, implying the particle can only move inside the pockets in this cluster.

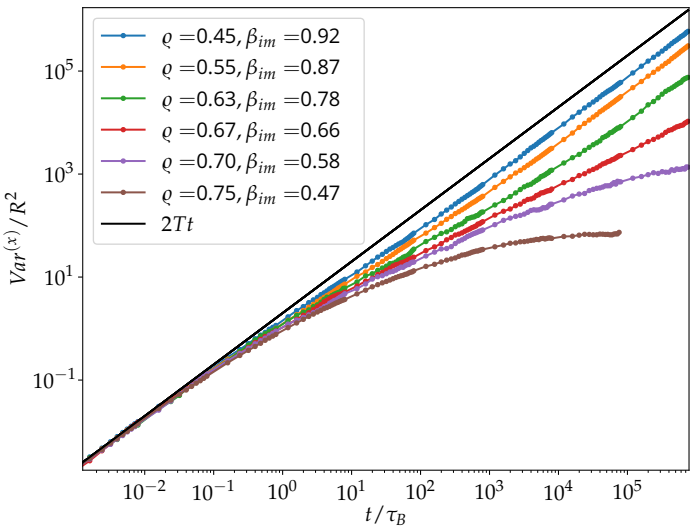

Figure 3.2: The variance of the position $Var^{(x)}(t)$ and the exponent of anomalous diffusion for intermediate times β_{im} of a non-driven particle in a disordered medium is shown for different densities ϱ. For comparison, the figure also shows the variance for free diffusion $2Tt$ in black. The exponent of anomalous diffusion β_{im} is calculated as a fit parameter in the equation $\ln(Var^{(x)}(t)) = \ln(2Dt^{\beta})$. The curve fit is only applied to data points in the time interval $(20\tau_B, 300\tau_B)$.

3.2.2 Effects of the driving force

In this section, we review the effects of the driving force f on a Brownian particle in a disordered medium. We start by briefly discussing the driving force's effect on the mobility v/f.
Consider a particle subject to a large driving force f and a comparably small noise strength $\sqrt{2T}$. The particle will get trapped at an obstacle's surface perpendicular to the driving force. This means that the trapping probability increases with an increase in driving force. Thus, the particle's mobility v/f will decrease with an increasing driving force f, as shown in Figure 3.3 for two specific densities. The figure also shows that the mobility decreases with increasing density ϱ.

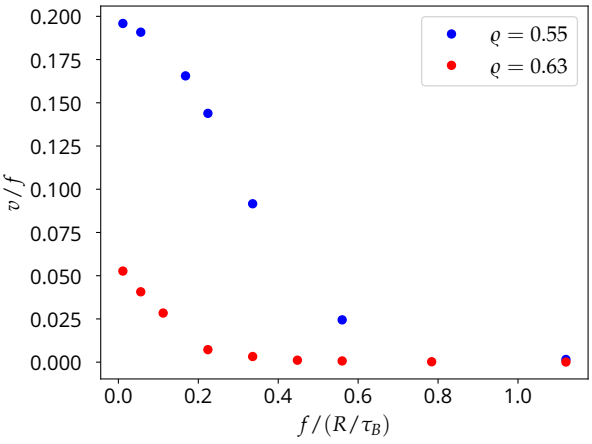

Figure 3.3: This figure shows the mobility v/f versus the driving force f for driven Brownian particles in a disordered medium with obstacle densities $\varrho = 0.55$ and $\varrho = 0.63$. The average velocity v is calculated as a fit parameter in the equation $\ln(\langle x \rangle) = \ln(vt)$. The curve fit is only applied to data points in the time interval $(10^5\tau_B, 10^6\tau_B)$, see Section 3.1.

We resume by discussing how the variance $Var^{(x)}$ and the uncertainty product Q for a constant density depend on the driving force. $Var^{(x)}(t)$ is shown for different values of f at a constant density $\varrho = 0.63$ in Figure 3.4. For very small driving forces (e.g. $f = 0.0112R/\tau_B$ shown in blue) the variance $Var^{(x)}(t)$ remains almost unchanged compared to $f = 0$. For slightly larger driving forces (e.g. $f = 0.112R/\tau_B$ shown in orange) the dynamics are superdiffusive for long time scales. This effect has been described in e.g. [59, 62], even though it is important to note that they use slightly different geometries than us (dumbbell-shaped obstacles and circular obstacles inside a symmetric channel). Superdiffusive behavior for a driven continuous-time random walk on a Lorentz gas lattice has been reported as well [63]. For high driving forces, such as $f = 1.12R/\tau_B$ shown in green, the trapping effect due to the driving force is strong, but the particles show superdiffusion ($\beta = 1.2$) for long times.
As described at the beginning of this section, increasing the driving force f leads to the particle's trapping against the obstacle's surface. This restricts the particle's movement reducing the variance of position compared to the non-driven particle. If f is significantly bigger than the noise, particles will often be completely trapped. This effect has been described e.g., by [35] and [59]. Another consequence of an increased driving force f is the faster movement through the free space, which results in the earlier occurrence of subdiffusion.
In comparison to Figure 3.4 the corresponding uncertainty products $Q(t)$ are shown in Figure 3.5. For $f = 0.0112R/\tau_B$ (blue) $Q(t)$ decreases over time approaching $Q = 2$ for long times. For $f = 0.112R/\tau_B$ (orange) superdiffusion for long times leads to an increase in Q. For $f = 1.12R/\tau_B$ (green) an increase in Q for long times (superdiffusion) can be seen as well. Figure 3.6 shows the minimal uncertainty product $Q_{min} = min_t Q(t)$ versus the driving force f for two densities $\varrho = 0.55$ (blue) and $\varrho = 0.63$ (red). The uncertainty product $Q \sim D/(v/f)$ increases with increasing f, this is due to the strong decrease in v/f.
In Figure 3.7 the minimal uncertainty product Q_{min} versus the driving force f is shown for small values of f. Even though the TUR becomes an increasingly tight bound with decreasing f, a violation of the TUR in the small f regime can not be anticipated from this data.
It is well known that the TUR is tight for systems close to equilibrium [9, 11, 64].

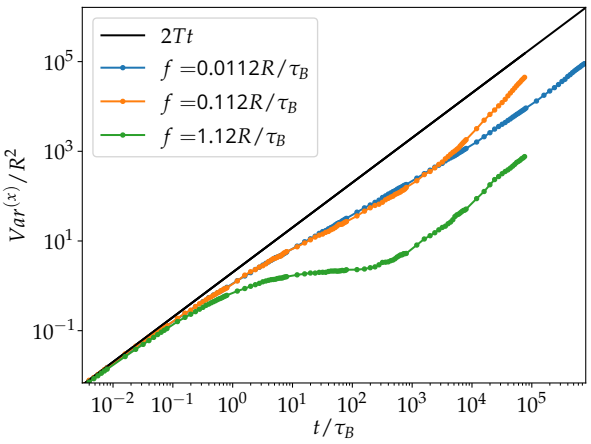

Figure 3.4: The variance of the position $Var^{(x)}(t)$ of the driven Brownian particle in a disordered medium is shown for density $\varrho = 0.63$ and for driving forces $f/(R/\tau_B) \in \{0.0112, 0.112, 1.12\}$. For comparison, the figure also shows the variance for free diffusion $2Tt$ in black.

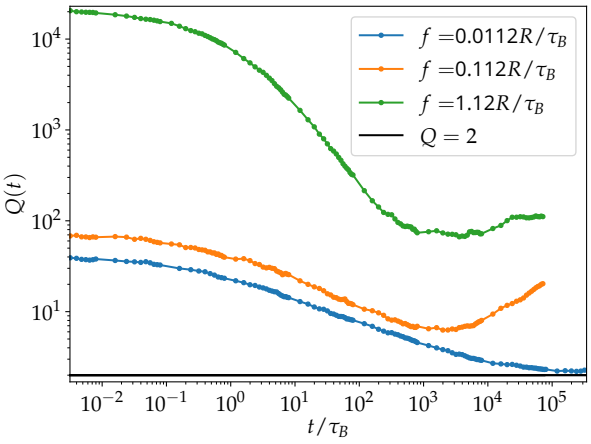

Figure 3.5: The uncertainty product $Q(t)$ for density $\varrho = 0.63$ and driving force $f/(R/\tau_B) \in \{0.0112, 0.112, 1.12\}$ is shown. For comparison, the figure also shows the lower bound $Q = 2$ given by the TUR in black. Note that both axes are scaled logarithmically.

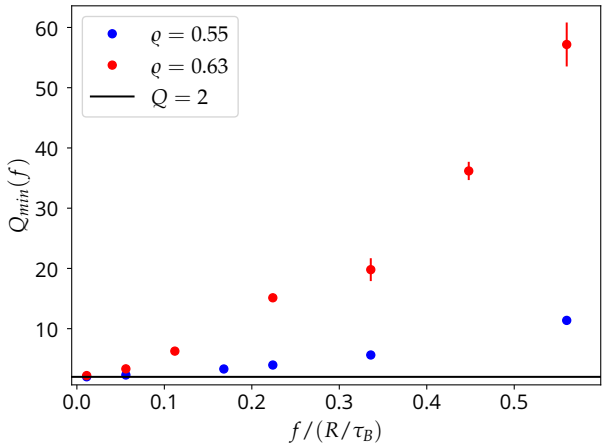

Figure 3.6: Minimal uncertainty product Q_{min} versus f for densities $\varrho = 0.55$ and $\varrho = 0.63$. For comparison, the figure also shows the lower bound $Q = 2$ given by the TUR in black. The measurement uncertainties (error bars) are given by the deviation of the minimal value from the average of its five surrounding values, as described in Section 2.3.3.

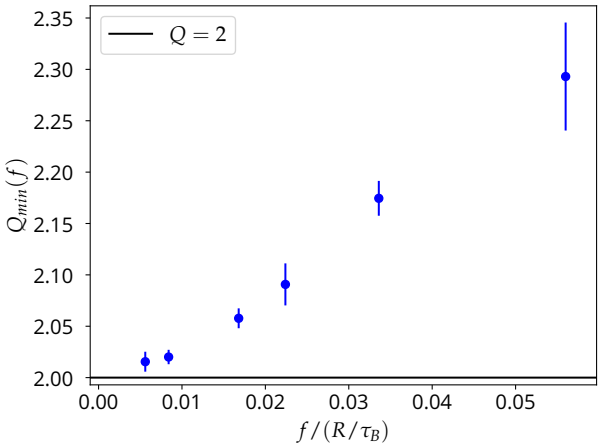

Figure 3.7: Minimal uncertainty product Q_{min} versus the driving force f for density $\varrho = 0.55$ and small values of f. For comparison, the figure also shows the lower bound $Q = 2$ given by the TUR. The measurement uncertainties (error bars) are given by the deviation of the minimal value from the average of its five surrounding values.

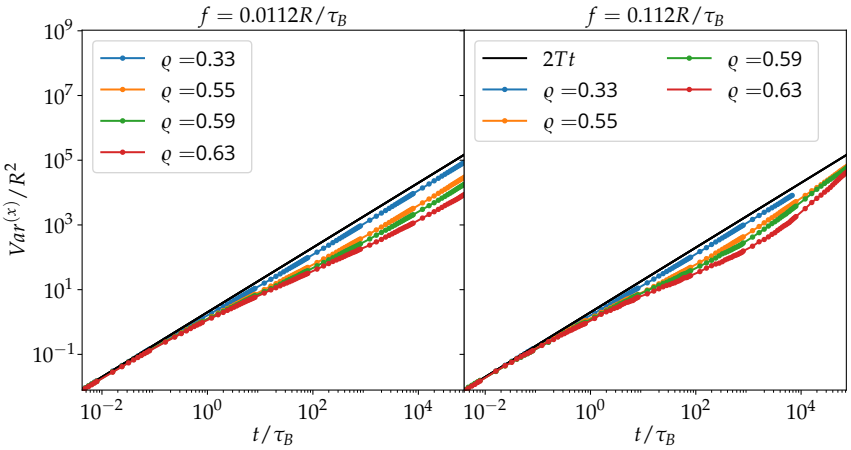

Figure 3.8: The variance of the position $Var^{(x)}(t)$ of the driven Brownian particle in a disordered medium is shown for densities $\varrho \in \{0.33, 0.55, 0.59, 0.63\}$ and driving forces $f = 0.0112R/\tau_B$ (left) and $f = 0.112R/\tau_B$ (right) in comparison with the variance for free diffusion $2Tt$.

3.2.3 Uncertainty product affected by the density

In this section, we evaluate the previously discussed results from a different point of view. We compare different densities ϱ while the driving force f is constant. We start by reviewing the variance $Var^{(x)}(t)$.
For small f we see the variance growing linear for long times, see Figure 3.8 left. As we saw in the non-driven case, the diffusion coefficient decreases with increasing density. For larger f and small densities (e.g. $\varrho = 0.33$) the variance also grows linear for long times, see Figure 3.8 right. But as described in the previous section, we observe superdiffusive behavior for larger densities.
As can be seen in Figure 3.3 the mobility decreases with increasing density. In Figure 3.9 it can be seen that Q_{min} increases with an increase in the density. We know that the TUR is tight ($Q = 2$) for diffusion in free space $\varrho = 0$, see Section 1.3.1.

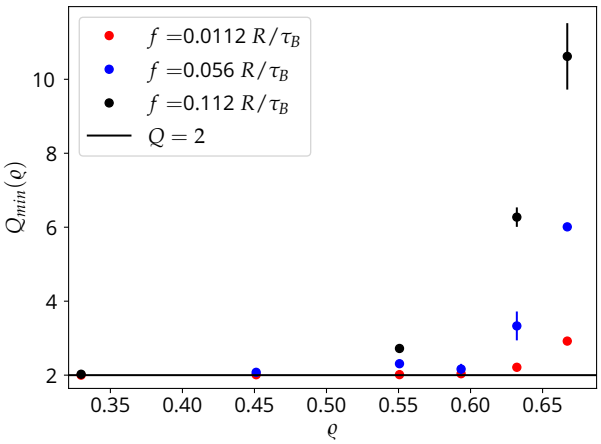

Figure 3.9: Minimal uncertainty product Q_{min} versus the density ϱ for $f/(R/\tau_B) \in \{0.0112, 0.055, 0.112\}$ in different colors. For comparison, the figure also shows the lower bound $Q = 2$ given by the TUR in black. The measurement uncertainties (error bars) are given by the deviation of the minimal value from the average of its five surrounding values.

3.2.4 Effects of anisotropic noise

In this section, we investigate the effect of anisotropic noise on Q. As Equation (1.36) describes, the TUR states that $D/T \geq v/f$. Thus the TUR dictates that a decrease in the diffusion coefficient leads to a decrease in mobility. One way of decreasing the diffusion coefficient, investigated in Section 3.2.3, is by increasing the obstacle density.

In this section, we choose different noise strengths in x- and y-direction. We investigate the influence of such a choice of noise intensities on subdiffusion and the TUR. The Langevin equation (3.1) is thus modified to

$$\dot{x} = f + \sqrt{2T_x}\xi_x(t), \tag{3.8}$$

$$\dot{y} = \sqrt{2T_y}\xi_y(t). \tag{3.9}$$

In the following we use the notation $T_x = T$. As for isotropic noise, we employ the Cichocki-Hinsen algorithm and the Euler-Maruyama scheme. The trapping probability against an obstacle's surface increases with a decrease in the noise strength in y-direction. For high T_y the particle diffuses very quickly around the obstacles.

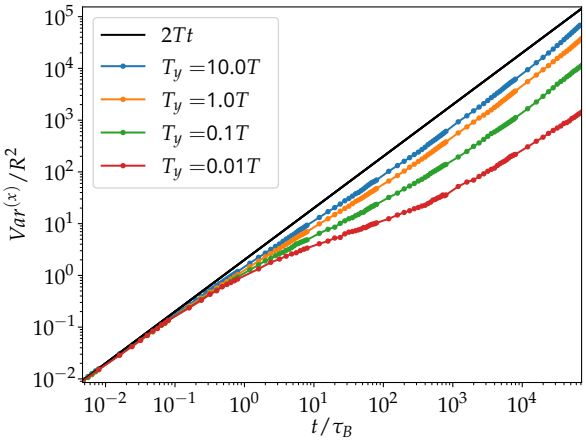

Figure 3.10: The variance of the position $Var^{(x)}(t)$ of a driven Brownian particle in a disordered medium with anisotropic noise ($T_y/T \in \{0.01, 0.1, 1, 10\}$) is shown for density $\varrho = 0.55$ and driving force $f = 0.056R/\tau_B$ in comparison with the variance for free diffusion $2Tt$.

In Figure 3.10 the variance $Var^{(x)}(t)$ is shown for different temperatures T_y in y-direction. The figure shows that an increase in T_y leads to a higher diffusion coefficient (with respect to x) and a decrease in T_y leads to a lower diffusion coefficient (with respect to x) and a prolonged subdiffusion. Figure 3.11 shows the mobility v/f versus T_y. As one expects, v/f grows with increasing T_y.
Since the mobility v/f decreases so strongly for low T_y, the uncertainty product Q_{min} grows, as seen in Figure 3.12. For high T_y the particles quickly diffuse through the medium, approaching free diffusion ($Q = 2$).

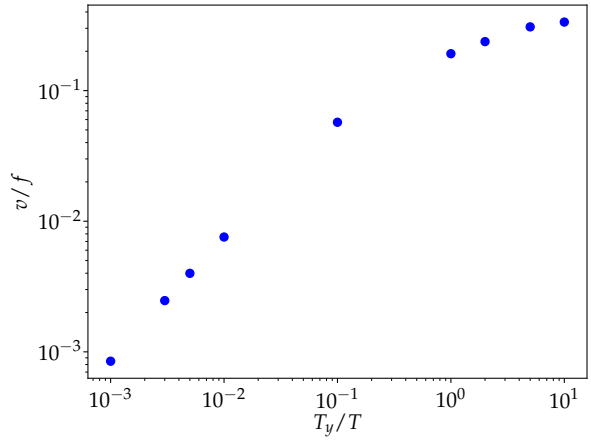

Figure 3.11: The mobility v/f of a driven Brownian particle in a disordered medium with anisotropic noise is shown versus the temperature T_y in y-direction for $\varrho = 0.55$ and $f = 0.056R/\tau_B$.
The mean velocity is calculated as a fit parameter from the equation $\ln(\langle x \rangle) = vt$.

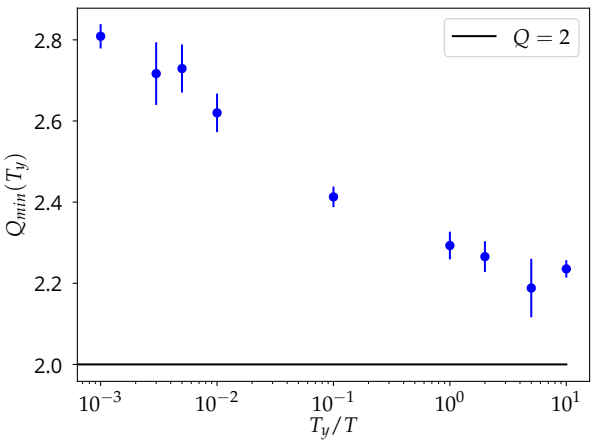

Figure 3.12: The minimal uncertainty product Q_{min} is shown versus the temperature T_y in y-direction for $\varrho = 0.55$ and $f = 0.056R/\tau_B$. The measurement uncertainties (error bars) are given by the deviation of the minimal value from the average of its five surrounding values.

3.2.5 Comparison with CTRW results

The continuous-time random walk (CTRW) [30] is a mathematical model for anomalous diffusion [31]. In a one-dimensional CTRW, the particle with position x jumps after a random waiting time τ. The waiting time is drawn from a waiting time distribution (WTD) $\psi(\tau)$. The jumps can have a fixed length for simplicity and the two directions (right and left) have the probabilities p and $q = 1 - p$ respectively.
In [31], Hou et al. considered different WTDs for which the particle exhibits various kinds of diffusion. We now discuss their results to compare anomalous diffusion in the CTRW model to the disordered medium. If $p \neq q$ the particle is driven. In a steady state, the mean position will then grow linear in time $\langle x \rangle \sim (p - q)t$. We consider a power-law WTD

$$\psi(\tau) \sim \tau^{-1-\alpha}. \tag{3.10}$$

We now review the TUR for the CTRW results. As Equation (1.31) states, we can rewrite the TUR as $Q \sim Var^{(x)}/\langle x \rangle \geq$ constant.

Table 3.1: Variance $Var^{(x)}$ and uncertainty product Q for CTRWs with different WTD exponents α. The results for the variance are taken from [31].

WTD exponent	$Var^{(x)}(t)$	small time Q	long time Q
$\alpha > 2$	$\sim t$	const.	const.
$1 < \alpha < 2$	$\sim \mathcal{O}(t) + (p-q)^2\mathcal{O}(t^{3-\alpha})$	const.	$\sim t^{2-\alpha}$
$0 < \alpha < 1$	$\sim \mathcal{O}(t^{\alpha}) + (p-q)^2\mathcal{O}(t^{2\alpha})$	$\sim t^{\alpha-1}$	$\sim t^{2\alpha-1}$

As we can see from Equation (3.10) for the first two cases ($1 < \alpha$) listed in Table 3.1, the mean waiting time

$$\int_0^{\infty} \tau\psi(\tau)d\tau \tag{3.11}$$

converges. For those cases we only see normal and (driving force-induced) superdiffusion and the TUR remains valid. In the third case $0 < \alpha < 1$ we observe subdiffusion if $\alpha < 1/2$ for all times and if $1/2 < \alpha$ for small times. For small times $Q(t)$ decreases for $0 < \alpha < 1$. It then is a matter of prefactors whether the TUR remains valid. For long times $Q(t)$ decreases if $\alpha < 1/2$ and the TUR will be violated. If $\alpha > 1/2$, the TUR remains valid for long times.
In Sections 2.3.3 and 3.2 the numerical results of the simulations did not show a violation of the TUR. The results of both models showed a linearly growing variance for (very) small times, see Figures 2.4 and 3.4. Thus, our numerical results show different behavior than the CTRW results with $0 < \alpha < 1$.

3.3 Calculating the mean covered area

Consider a geometric object with an area A randomly placed in a larger area B. Ignoring boundary effects, the object will cover the area fraction $X = A/B$. Consider a second identical object randomly placed in B. The two objects will on average not cover $2X$ of B now. But instead, $X + X(1 - X)$, since the second object can only cover previously uncovered area.

For any number of objects N, we define the mean covered area fraction as ϱ_N. The recursion equation states

$$\varrho_{N+1} = \varrho_N + X(1 - \varrho_N). \tag{3.12}$$

The sequence

$$\varrho_N = 1 - (1 - X)^N = 1 - \left(1 - \frac{XN}{N}\right)^N \tag{3.13}$$

satisfies the equation above.
For the limit of $N \to \infty$ we see $\varrho_N \to 1 - e^{-XN}$, in agreement with [60]. On the other hand, for the limit $XN \to 0$, we find $\varrho_N = XN$, the result for non-overlapping geometric objects.

4 Underdamped two-dimensional Model

In this final chapter, we investigate the behavior of underdamped Brownian particles in a disordered medium. Unlike in the previous chapters, where thermodynamics was decribed for overdamped systems, the TUR is known not to be valid for underdamped systems [43]. In Section 4.1, we will discuss the well-known behavior of underdamped particles in free space and the uncertainty product for driven underdamped particles in free space. We will then discuss the model used for the simulations in Section 4.2. Finally, the numerical results for underdamped particles are described in Section 4.3. As expected, we find a violation of the TUR for driven underdamped particles at different times.

4.1 Underdamped particles in free space

4.1.1 Free diffusion of underdamped particles

Referring back to Section 1.1.1, using $\gamma = 1$ and $k_B = 1$ and following the example given by [15], an underdamped particle, with no external force acting on it, is described by the Langevin equation

$$\begin{aligned} m\ddot{x} &= -\dot{x} + \sqrt{2T}\xi(t) \\ \Leftrightarrow m\dot{v} &= -v + \sqrt{2T}\xi(t). \end{aligned} \tag{4.1}$$

Here $v = \dot{x}$ is the velocity of the particle at a time and does not denote the mean velocity as in Chapters 2 and 3. If we assume the particle is initially at rest $v(t = 0) = 0$, the solution of the Langevin equation is

$$v(t) = \int_0^t \exp\left[-(t - t')/m\right] \frac{\sqrt{2T}}{m} \xi(t')dt'. \tag{4.2}$$

This can be verified by the Leibniz integral rule. We then calculate the velocity autocorrelation for δ-correlated noise

$$\begin{aligned} \langle v(t_1)v(t_2)\rangle &= \frac{2T}{m^2} \int_0^{t_1} \int_0^{t_2} \exp\left[-(t_1 + t_2 - t_1' - t_2')/m\right] \langle \xi(t_1')\xi(t_2')\rangle dt_2' dt_1' \\ &= \frac{2T}{m^2} \int_0^{t_1} \exp\left[-(t_1 + t_2 - 2t_1')/m\right] dt_1' \\ &= \frac{T}{m}\Big(\exp[(t_1 - t_2)/m] - \exp[-(t_1 + t_2)/m]\Big). \end{aligned} \tag{4.3}$$

Since the velocity autocorrelation has to be symmetric under permutations of t_1 and t_2 and since

we consider the steady state, $t_1/m \gg 1$ and $t_2/m \gg 1$, we can rewrite

$$\langle v(t_1)v(t_2)\rangle = \frac{T}{m}\exp[-|t_2 - t_1|/m]. \tag{4.4}$$

For the $MSD^{(x)}$ (or equivalently the variance, since $\langle x(t) - x_0\rangle = 0$) we calculate

$$\begin{aligned} MSD^{(x)}(t) &= \left\langle (x(t) - x_0)^2 \right\rangle = \left\langle \int_0^t v(t_1)dt_1 \int_0^t v(t_2)dt_2 \right\rangle \\ &= \int_0^t \int_0^t \langle v(t_1)v(t_2)\rangle \, dt_1 dt_2 = 2\int_0^t \int_0^{t_2} \langle v(t_1)v(t_2)\rangle \, dt_1 dt_2 \\ &= 2\frac{T}{m}\int_0^t \int_0^{t_2} \exp[-|t_2 - t_1|/m]dt_1 dt_2 = 2T\int_0^t (1 - \exp[-t_2/m])dt_2 \\ &= 2Tt + 2Tm(\exp[-t/m] - 1). \end{aligned} \tag{4.5}$$

From this we can readily identify two limits.
First, for $t/m \gg 1$, meaning either $m \to 0$ or $t \to \infty$, we obtain the overdamped limit $MSD^{(x)}(t) = 2Tt$. Second, at small times we can approximate the exponential function by the Taylor series of second order

$$MSD^{(x)}(t) \approx 2Tt + 2Tm\left(1 - \frac{t}{m} + \frac{t^2}{2m^2} + \mathcal{O}\left(t^3\right) - 1\right) = \frac{T}{m}t^2 + \mathcal{O}\left(t^3\right). \tag{4.6}$$

This means for small times the $MSD^{(x)}$ (or equivalently the variance) will grow ballistically for underdamped particles.

4.1.2 Driven underdamped particles

In this section, we calculate the average velocity of a driven underdamped Brownian particle in free space. With a constant driving force, the particle's dynamics are described by the Langevin equation

$$m\dot{v} = f - v + \sqrt{2T}\xi. \tag{4.7}$$

We consider the ensemble average, which leads to the differential equation

$$m\langle\dot{v}\rangle = f - \langle v\rangle \tag{4.8}$$

and its solution to the initial condition $\langle v\rangle(t = 0) = u_0$ is

$$\langle v\rangle(t) = u_0 e^{-t/m} + f. \tag{4.9}$$

For both $t \to \infty$ and $m \to 0$ we identify the underdamped limit

$$\lim_{t\to\infty} \langle v\rangle(t) = f. \tag{4.10}$$

4.1.3 Thermodynamic uncertainty relation for underdamped particles

It is shown in several systems that underdamped dynamics are not constrained by the TUR [43, 44, 65]. Following the example given by Fischer et al. in [65], we will briefly discuss the uncertainty product Q of an underdamped particle with mass m subject to a constant driving force f in free space. For the uncertainty product Q, they obtained

$$Q(t) = \frac{2m}{t}\left(\frac{t}{m} + \exp(-t/m) - 1\right). \tag{4.11}$$

For long times or small masses, $t/m \gg 1$, we identify the limit $Q = 2$. This is equal to what we find for an overdamped driven Brownian particle in free space, see Section 1.3.1. For small times the exponential function can be approximated by a Taylor series of second order and we obtain

$$Q(t) = \frac{2m}{t}\left(\frac{t}{m} + 1 - \frac{t}{m} + \frac{t^2}{2m^2} + \mathcal{O}\left(t^3\right) - 1\right) = \frac{t}{m} + \mathcal{O}\left(t^2\right). \tag{4.12}$$

This means the variance of the position is only constrained by the TUR at long times. The TUR is violated at short times.
Recently a system was investigated where the TUR was violated for infinite times as well [66]. In this system, an underdamped driven Brownian particle moves in a harmonic potential with an additional potential. The potential is coupling the x- and y-directions. The particle acts as a classical pendulum clock with an escapement mechanism.

4.2 Model

The model we use for the underdamped particles is very similar to the model described in Section 3.1. The only difference is the consideration of the inertial effect and a different integration scheme. The particle has mass m and the Langevin equation thus reads

$$m\ddot{\vec{r}} = -\dot{\vec{r}} + f\vec{e}_x + \sqrt{2T}\vec{\xi}(t). \tag{4.13}$$

The Chikochi-Hinsen algorithm is employed again to model the obstacle-tracer interaction. The Langevin equation is integrated numerically using a Verlet-type algorithm [48] which is based on the Verlet algorithm [67].
If we consider a Langevin equation with an external force F

$$m\dot{v} = -v + F(x,t) + \eta(t), \quad \dot{x} = v \tag{4.14}$$

the algorithm reads

$$\begin{aligned} x_{n+1} &= x_n + b\,dt\,v_n + \frac{b\,dt^2}{2m}F_n + \frac{b\,dt}{2m}\tilde{\eta}_{n+1}, \\ v_{n+1} &= av_n + \frac{dt}{2m}(aF_n + F_{n+1}) + \frac{b}{m}\tilde{\eta}_{n+1}, \\ a &= \frac{1-\frac{dt}{2m}}{1+\frac{dt}{2m}}, \quad b = \frac{1}{1+\frac{dt}{2m}}. \end{aligned} \tag{4.15}$$

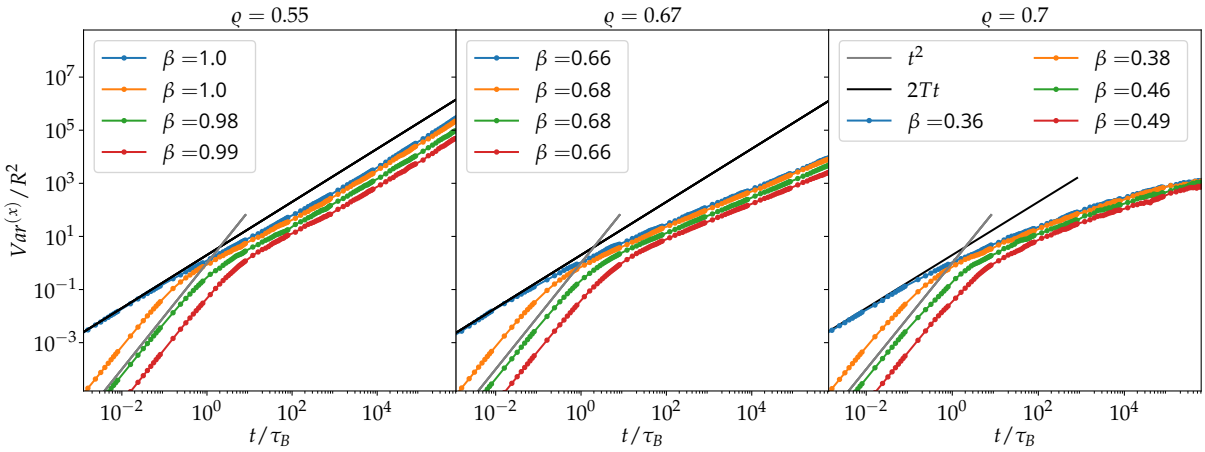

Figure 4.1: The variance of the position $Var^{(x)}(t)$ and the long-time exponent of anomalous diffusion β for over- and underdamped non-driven particles in a disordered medium are shown. The masses shown are $m = 0$ (overdamped) in blue, $m = 0.0797\tau_B$ in orange, $m = 0.797\tau_B$ in green and $m = 3.99\tau_B$ in red. On the left hand side we show the density $\varrho = 0.55$, in the center $\varrho = 0.67$ and on the right hand side $\varrho = 0.7$. For comparison the variance of an overdamped particle in free space $Var^{(x)}(t) = 2Tt$ (black) and the small-time variance $Var^{(x)}/R^2 = t^2/\tau_B^2$ of an underdamped particle with mass $m = 1\tau_B$ (gray) is shown. The long-time exponent of anomalous diffusion β is calculated as a fit parameter in the equation $\ln(Var^{(x)}(t)) = \ln(2Dt^\beta)$. The curve fit is only applied to data points with time $t \in (10^5\tau_B, 10^6\tau_B)$.

Here, the indices denote the corresponding iteration and $F_n = F(x_n, t_n)$. Note that unlike in Chapters 2 and 3, the numerical values of the noise $\tilde{\eta}$ have a variance of $\sqrt{2T\Delta t}$ where Δt is the numerical time step [48].

4.3 Results

4.3.1 Subdiffusion of underdamped non-driven particles

First, we review the subdiffusion for underdamped particles, meaning $f = 0$. The variance $Var^{(x)}(t)$ for masses $m/\tau_B \in \{0, 0.0797, 0.797, 3.99\}$ (in blue, orange, green and red) and densities $\varrho \in \{0.55, 0.67, 0.7\}$ (left, center, right) is shown in Figure 4.1. In agreement with the calculations from Section 4.1.1, we see a ballistic behavior of the variance for underdamped particles for small times $Var^{(x)}(t) \sim t^2$. For small densities (left) the particles diffuse normally for long times. Around the percolation limit $\varrho = 0.67$ (center) the exponents of anomalous diffusion of the underdamped particles with different masses and the overdamped particles are similar. This makes sense since the percolation limit is an entirely geometric property of the space in which the particles can move. For higher densities (right) the variance saturates.
For all examined densities, we find the variance of the overdamped particles to provide an upper limit for the variances of the underdamped particles.

4.3.2 Underdamped driven particles

We now resume with the variance of driven particles. In Figure 4.2 (top) the variance of over- and underdamped particles with $\varrho = 0.55$ and driving forces $f = 0.0112R/\tau_B$ (left) and $f = 0.056R/\tau_B$ (right) is shown.
For $f = 0.0112R/\tau_B$, the diffusion is approximately normal for long times ($\beta \approx 1$). The diffusion coefficient decreases with an increase in mass. For $f = 0.056R/\tau_B$, all particles regardless of

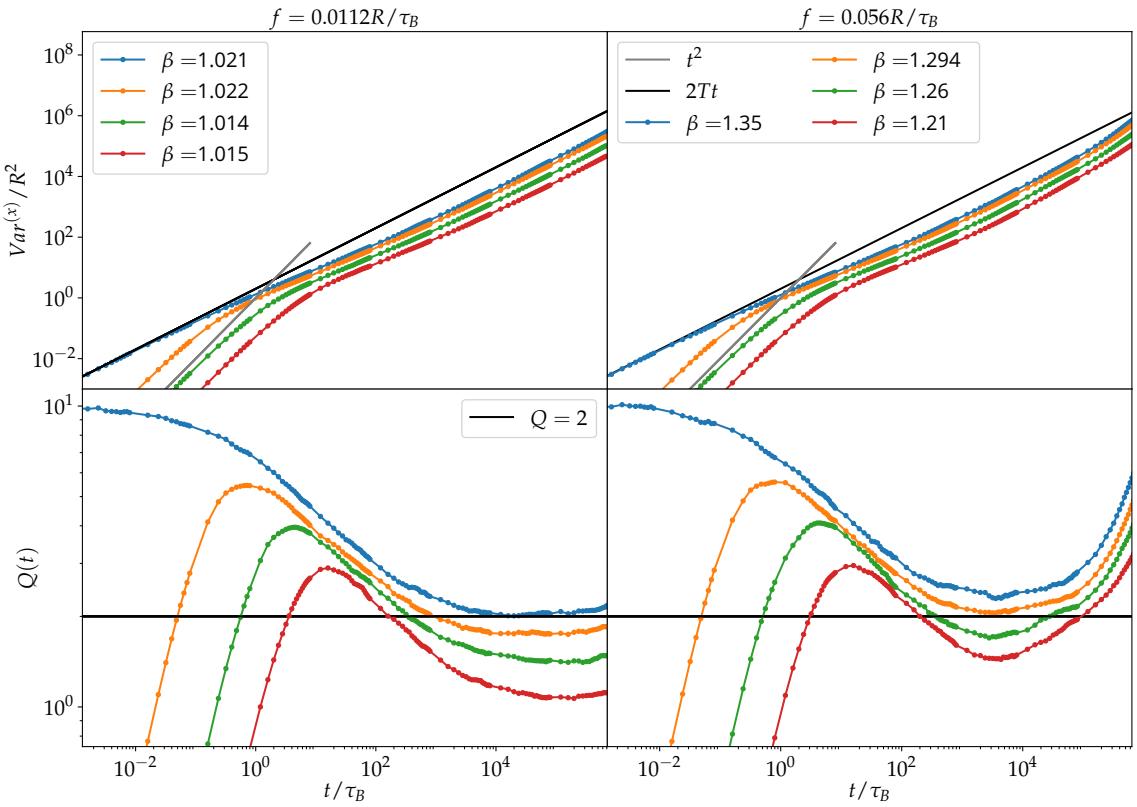

Figure 4.2: The variance of the position $Var^{(x)}(t)$ and the long-time exponent of anomalous diffusion β (top) and the uncertainty product $Q(t)$ (bottom) are shown for over- and underdamped driven particles in a disordered medium with density $\varrho = 0.55$. The masses shown are $m = 0$ (overdamped) in blue, $m = 0.0797\tau_B$ in orange, $m = 0.797\tau_B$ in green and $m = 3.99\tau_B$ in red. On the left hand side we show the driving force $f = 0.0112R/\tau_B$ and on the right hand side $f = 0.056R/\tau_B$. For comparison, in the top graphs the variance of an overdamped particle in free space $Var^{(x)}(t) = 2Tt$ (black) and the small-time variance $Var^{(x)}/R^2 = t^2/\tau_B^2$ of an underdamped particle with mass $m = 1\tau_B$ (gray) is shown, in the bottom graphs the lower bound of the uncertainty product $Q = 2$ given by the TUR is shown in black. The long-time exponent of anomalous diffusion β is calculated as a fit parameter in the equation $\ln(Var^{(x)}(t)) = \ln(2Dt^\beta)$. The curve fit is only applied to data points with time $t \in (10^5\tau_B, 10^6\tau_B)$.

their mass show superdiffusive behavior at long times.
For all underdamped particles the expected ballistic behavior of the variance for small times is visible. Since the particles' mass is responsible for the initial effect, see Equation (4.5), the time of transition to normal or anomalous diffusion is mass-dependent. We find the variances to increase with a decrease in mass, converging towards the overdamped limit.
For the same parameters, we now review the uncertainty product. The corresponding uncertainty products $Q(t)$ are shown in the bottom graphs of Figure 4.2. As shown in this figure, the uncertainty product decreases with an increase in mass. This is equivalent to the observation that an increase in mass decreases the variance stronger than it decreases the mobility v/f. For masses $m \geq 0.07\tau_B$, we find a violation of the TUR for $f = 0.0112R/\tau_B$. For $f = 0.056R/\tau_B$ the TUR is violated for transient times for masses $m \geq 0.7\tau_B$.
Since we found $\beta \approx 1$ for the small driving force $f = 0.0112R/\tau_B$, see Figure 4.2 (top left), the uncertainty product Q appears to be constant for long times. For all masses shown, the TUR would then be violated for long times.
For $f = 0.056R/\tau_B$ we found $\beta > 1$. This leads to an increase in the uncertainty product over

time. Thus the TUR is only violated for finite times.
Since the superdiffusion (and thus β) increases with the driving force and we find $\beta = 1$ for non-driven particles, it makes sense that even for small driving forces (e.g. $f = 0.0112R/\tau_B$) the exponent of anomalous diffusion β is slightly greater than 1. A slight increase in the uncertainty product Q can be seen for times $t \geq 10^5\tau_B$ for $f = 0.0112R/\tau_B$. The data is too noisy to make a clear claim. But if this were true, the times we calculated would not be long enough to show true long-time behavior. This would mean that the TUR would also only be violated for transient times in this case ($f = 0.0112R/\tau_B$). This of course does not mean that the TUR could not be violated for a different set of parameters for infinite times in a crowded environment.

4.3.3 Anisotropic noise

We also investigate the influence of anisotropic noise on the underdamped particles in the disordered medium. Figure 4.3 shows the variance (top) and the uncertainty product (bottom) for different masses with density $\varrho = 0.55$ and driving forces $f = 0.0112R/\tau_B$ (left) and $f = 0.056R/\tau_B$ (right) for anisotropic noise with $T_y = 0.01T$.
Similar to our findings in the overdamped case, see Section 3.2.4, we find a prolonging of subdiffusion due to the decrease in T_y. Even though the trajectories described in this and the previous section are all calculated for the same times, the long time effects observed in the previous section can not be seen in the trajectories described in this section. For example consider the driving force $f = 0.0112R/\tau_B$. Using isotropic noise, the particles diffuse normally at the end of their recorded trajectories. On the other hand, using $T_y = 0.01T$, the particles show the transition to normal diffusion at the same time, see Figure 4.3 top left. This effect can be observed for all masses and driving forces we considered.
The second important effect is the increase of the uncertainty product, which is explained by the strong decrease in the particles' mobility. This also agrees with our findings from the overdamped case, see Figure 3.12. One example to illustrate this is given by the particles driven by $f = 0.056R/\tau_B$. While the TUR is violated for $m \geq 1\tau_B$ when using isotropic noise, as described in the previous section, the TUR is not violated for masses up to $m = 5\tau_B$ when using $T_y = 0.01T$. This can be seen comparing the bottom right plots of Figures 4.2 and 4.3.

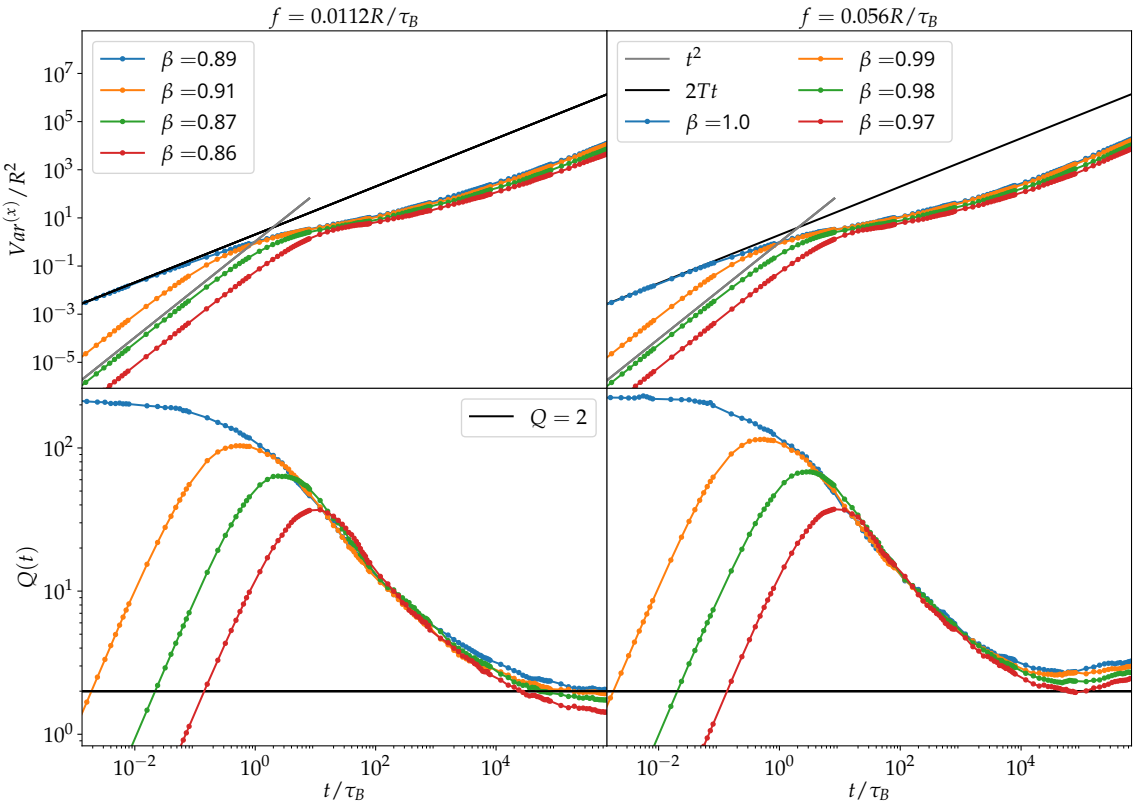

Figure 4.3: The variance of the position $Var^{(x)}(t)$ and the long-time exponent of anomalous diffusion β (top) and the uncertainty product $Q(t)$ (bottom) are shown for over- and underdamped driven particles in a disordered medium with density $\varrho = 0.55$. Unlike in Figure 4.2 here we deal with anisotropic noise, where $T_y = 0.01T$. The masses shown are $m = 0$ (overdamped) in blue, $m = 0.0797\tau_B$ in orange, $m = 0.797\tau_B$ in green and $m = 3.99\tau_B$ in red. On the left hand side we show the driving force $f = 0.0112R/\tau_B$ and on the right hand side $f = 0.056R/\tau_B$. For comparison in the top graphs the variance of an overdamped particle in free space $Var^{(x)}(t) = 2Tt$ (black) and the small-time variance $Var^{(x)}/R^2 = t^2/\tau_B^2$ of an underdamped particle with mass $m = 1\tau_B$ (gray) is shown, in the bottom graphs the lower bound of the uncertainty product $Q = 2$ given by the TUR is shown in black. The long-time exponent of anomalous diffusion β is calculated as a fit parameter in the equation $\ln(Var^{(x)}(t)) = \ln(2Dt^{\beta})$. The curve fit is only applied to data points with time $t \in (10^5\tau_B, 10^6\tau_B)$.

5 Conclusion

In this thesis, we performed Brownian dynamics simulations to examine the thermodynamic uncertainty relation (TUR) for anomalous diffusion.
On the one hand, we studied overdamped particles in a one-dimensional trap model and compared our results to existing analytic expressions. The effective diffusion coefficient of non-driven particles was shown to agree with the Lifson-Jackson formula. Driven particles very clearly exhibited giant diffusion, which is an increase in the diffusion coefficient for specific driving forces. We found the TUR to be a tight bound only for small and high driving forces (compared to the potential strengths). In the limit of infinite driving forces, the particle diffuses in effectively free space and the TUR is thus a tight bound. For driving forces of the same order as the potential strength, the effect of giant diffusion loosens the bound of the TUR.
On the other hand, we studied over- and underdamped particles in a two-dimensional disordered medium. The disordered medium consists of randomly placed immobile circular solid obstacles. The Brownian particle's interaction with the obstacles was modeled via the Cichocki-Hinsen algorithm. For non-driven particles we identified the percolation limit $\varrho_c = 0.67$.
For overdamped driven particles, it was found that the particles diffuse normally for small driving forces. For larger driving forces the particles showed superdiffusive behavior; for very high driving forces, the particles got trapped at the obstacles' surface. The last effect leads to a strong decrease in the particles' mobility v/f when increasing the driving force f. For overdamped driven particles the TUR bounds the variance of position tightly for small driving forces, low obstacle densities ϱ and strong noises T_y perpendicular to the driving force. For the limits $\varrho \to 0$ and $T_y \gg T$, free diffusion is approached and for $f \to 0$, the system is close to equilibrium. For those two cases, it is known that the TUR provides a tight bound for $Var^{(x)}/\langle x \rangle$.
Finally, the examination of underdamped particles lead to the expected violation of the TUR. Due to the superdiffusive behavior of the driven particles, the uncertainty product was found to increase with time for the system parameters considered. This leads to a violation only for finite times.
Possible directions for future research could be finding an explanation for the superdiffusive behavior of driven particles in disordered media. This could have potential consequences on understanding transport processes in crowded biological media. The question of whether the TUR can be violated by underdamped particles in a crowded environment for infinite time has not been the focus of this work. However, it could be interesting to study this closer in the future. In general, a wider range of stochastic thermodynamics can be investigated for anomalous dynamics, be it generated by Markovian or non-Markovian processes.

Bibliography

[1] R. Ellis, "Macromolecular crowding: obvious but underappreciated", Trends in Biochemical Sciences **26**, 597–604 (2001).

[2] F. Höfling and T. Franosch, "Anomalous transport in the crowded world of biological cells", Rep. Prog. Phys. **76**, 046602 (2013).

[3] E. Fodor, C. Nardini, M. E. Cates, J. Tailleur, P. Visco, and F. van Wijland, "How far from equilibrium is active matter?", Phys. Rev. Lett. **117**, 038103 (2016).

[4] R. Kubo, "The fluctuation-dissipation theorem", Reports on Progress in Physics **29**, 255–284 (1966).

[5] H. B. Callen and T. A. Welton, "Irreversibility and generalized noise", Phys. Rev. **83**, 34–40 (1951).

[6] K. Sekimoto, "Langevin Equation and Thermodynamics", Progress of Theoretical Physics Supplement **130**, 17–27 (1998).

[7] U. Seifert, "Stochastic thermodynamics: principles and perspectives", Eur. Phys. J. B **64**, 423–431 (2008).

[8] U. Seifert, "Stochastic thermodynamics, fluctuation theorems and molecular machines", Rep. Prog. Phys. **75**, 126001 (2012).

[9] A. C. Barato and U. Seifert, "Thermodynamic uncertainty relation for biomolecular processes", Phys. Rev. Lett. **114**, 158101 (2015).

[10] T. R. Gingrich, J. M. Horowitz, N. Perunov, and J. L. England, "Dissipation bounds all steady-state current fluctuations", Phys. Rev. Lett. **116**, 120601 (2016).

[11] S. K. Manikandan, D. Gupta, and S. Krishnamurthy, "Inferring entropy production from short experiments", Phys. Rev. Lett. **124**, 120603 (2020).

[12] D. Hartich and A. Godec, "Thermodynamic uncertainty relation bounds the extent of anomalous diffusion", Phys. Rev. Lett. **127**, 080601 (2021).

[13] S. M. J. Khadem, R. Klages, and S. H. L. Klapp, "On the stochastic thermodynamics of fractional brownian motion", 10.48550/ARXIV.2205.15791, `10.48550/ARXIV.2205.15791` (2022).

[14] S. Saryal, H. M. Friedman, D. Segal, and B. K. Agarwalla, "Thermodynamic uncertainty relation in thermal transport", Phys. Rev. E **100**, 042101 (2019).

[15] H. Risken, "Langevin equations", in *The Fokker-Planck Equation*, 2nd edition (Springer Berlin, Heidelberg, 1989).

[16] R. Brown, "XXVII. A brief account of microscopical observations made in the months of june, july and august 1827, on the particles contained in the pollen of plants; and on the general existence of active molecules in organic and inorganic bodies", The Philosophical Magazine **4**, 161–173 (1828).

[17] A. Einstein, "Über die von der molekularkinetischen Theorie der Wärme geforderte Bewegung von in ruhenden Flüssigkeiten suspendierten Teilchen", Annalen der Physik **322**, 549–560 (1905).

[18] M. von Smoluchowski, "Zur kinetischen Theorie der Brownschen Molekularbewegung und der Suspensionen", Annalen der Physik **326**, 756–780 (1906).

[19] P. Langevin, "Sur la theorie du mouvement brownien", C. R. Acad. Sci. (Paris) **146**, 530–533 (1908).

[20] A. D. Fokker, "Die mittlere Energie rotierender elektrischer Dipole im Strahlungsfeld", Annalen der Physik **348**, 810–820 (1914).

[21] M. Planck, "Über einen Satz in der statistischen Dynamik", Sitzung der physikalisch-mathematischen Klasse, 324–341 (1917).

[22] I. M. Sokolov and J. Klafter, "From diffusion to anomalous diffusion: A century after Einstein's Brownian motion", Chaos: An Interdisciplinary Journal of Nonlinear Science **15**, 026103 (2005).

[23] G. Schütz, H. Schindler, and T. Schmidt, "Single-molecule microscopy on model membranes reveals anomalous diffusion", Biophysical Journal **73**, 1073–1080 (1997).

[24] L. Wawrezinieck, H. Rigneault, D. Marguet, and P.-F. Lenne, "Fluorescence correlation spectroscopy diffusion laws to probe the submicron cell membrane organization", Biophysical Journal **89**, 4029–4042 (2005).

[25] I. Y. Wong, M. L. Gardel, D. R. Reichman, E. R. Weeks, M. T. Valentine, A. R. Bausch, and D. A. Weitz, "Anomalous diffusion probes microstructure dynamics of entangled f-actin networks", Phys. Rev. Lett. **92**, 178101 (2004).

[26] C. M. Anderson, G. N. Georgiou, I. E. Morrison, G. V. Stevenson, and R. J. Cherry, "Tracking of cell surface receptors by fluorescence digital imaging microscopy using a charge-coupled device camera. low-density lipoprotein and influenza virus receptor mobility at 4 degrees c", Journal of Cell Science **101**, 415–425 (1992).

[27] P. Schwille, U. Haupts, S. Maiti, and W. W. Webb, "Molecular dynamics in living cells observed by fluorescence correlation spectroscopy with one- and two-photon excitation", Biophysical Journal **77**, 2251–2265 (1999).

[28] T. Feder, I. Brust-Mascher, J. Slattery, B. Baird, and W. Webb, "Constrained diffusion or immobile fraction on cell surfaces: a new interpretation", Biophysical Journal **70**, 2767–2773 (1996).

[29] I. M. Sokolov, "Models of anomalous diffusion in crowded environments", Soft Matter **8**, 9043–9052 (2012).

[30] E. W. Montroll and G. H. Weiss, "Random walks on lattices. ii", J. Math. Phys. **6**, 167–181 (1965).

[31] R. Hou, A. G. Cherstvy, R. Metzler, and T. Akimoto, "Biased continuous-time random walks for ordinary and equilibrium cases: facilitation of diffusion, ergodicity breaking and ageing", Phys. Chem. Chem. Phys. **20**, 20827–20848 (2018).

[32] B. B. Mandelbrot and J. W. Van Ness, "Fractional brownian motions, fractional noises and applications", SIAM Review **10**, 422–437 (1968).

[33] S. C. Kou and X. S. Xie, "Generalized langevin equation with fractional gaussian noise: subdiffusion within a single protein molecule", Phys. Rev. Lett. **93**, 180603 (2004).

[34] R. G. Cole and T. Keyes, "The velocity correlation function for the lorentz gas", J Stat Phys **51**, 275–289 (1988).

[35] M. Zeitz, K. Wolff, and H. Stark, "Active brownian particles moving in a random lorentz gas", Eur. Phys. J. E **40** (2017).

[36] B. Sung and A. Yethiraj, "Lateral diffusion of proteins in the plasma membrane: spatial tessellation and percolation theory", The journal of physical chemistry. B **112**, 143–9 (2008).

[37] U. Seifert, "Entropy production along a stochastic trajectory and an integral fluctuation theorem", Phys. Rev. Lett. **95**, 040602 (2005).

[38] S. Pigolotti, I. Neri, E. Roldán, and F. Jülicher, "Generic properties of stochastic entropy production", Phys. Rev. Lett. **119**, 140604 (2017).

[39] A. Dechant and S. Sasa, "Current fluctuations and transport efficiency for general langevin systems", Journal of Statistical Mechanics: Theory and Experiment **2018**, 063209 (2018).

[40] K. Liu, Z. Gong, and M. Ueda, "Thermodynamic uncertainty relation for arbitrary initial states", Phys. Rev. Lett. **125**, 140602 (2020).

[41] P. Pietzonka, A. C. Barato, and U. Seifert, "Universal bounds on current fluctuations", Phys. Rev. E **93**, 052145 (2016).

[42] C. Dieball and A. Godec, "Direct route to thermodynamic uncertainty relations", `10.48550/ARXIV.2208.06402` (2022).

[43] T. Van Vu and Y. Hasegawa, "Uncertainty relations for underdamped langevin dynamics", Phys. Rev. E **100**, 032130 (2019).

[44] H.-M. Chun, L. P. Fischer, and U. Seifert, "Effect of a magnetic field on the thermodynamic uncertainty relation", Phys. Rev. E **99**, 042128 (2019).

[45] J.-M. Park and H. Park, "Thermodynamic uncertainty relation in the overdamped limit with a magnetic lorentz force", Phys. Rev. Research **3**, 043005 (2021).

[46] A. A. S. Kalaee, A. Wacker, and P. P. Potts, "Violating the thermodynamic uncertainty relation in the three-level maser", Phys. Rev. E **104**, L012103 (2021).

[47] G. Maruyama, "Continuous markov processes and stochastic equations", Rendiconti del Circolo Matematico di Palermo **4**, 48–90 (1955).

[48] N. Grønbech-Jensen and O. Farago, "A simple and effective verlet-type algorithm for simulating langevin dynamics", Molecular Physics **111**, 983–991 (2013).

[49] J. J. More, "Levenberg–marquardt algorithm: implementation and theory", Conference: Conference on numerical analysis, Dundee, UK, 28 Jun 1977 (1977).

[50] S. Lifson and J. L. Jackson, "On the self-diffusion of ions in a polyelectrolyte solution", The Journal of Chemical Physics **36**, 2410–2414 (1962).

[51] P. Reimann, C. Van den Broeck, H. Linke, P. Hänggi, J. M. Rubi, and A. Perez-Madrid, "Giant acceleration of free diffusion by use of tilted periodic potentials", Phys. Rev. Lett. **87**, 010602 (2001).

[52] A. M. Berezhkovskii and L. Dagdug, "Biased diffusion in periodic potentials: three types of force dependence of effective diffusivity and generalized lifson-jackson formula", The Journal of Chemical Physics **151**, 131102 (2019).

[53] U. Choudhury, A. V. Straube, P. Fischer, J. G. Gibbs, and F. Höfling, "Active colloidal propulsion over a crystalline surface", New J. Phys. **19**, 125010 (2017).

[54] L. Dagdug and A. M. Berezhkovskii, "Drift and diffusion in periodic potentials: upstream and downstream step times are distributed identically", The Journal of Chemical Physics **131**, 056101 (2009).

[55] G Costantini and F Marchesoni, "Threshold diffusion in a tilted washboard potential", Europhysics Letters (EPL) **48**, 491–497 (1999).

[56] P. Reimann, C. Van den Broeck, H. Linke, P. Hänggi, J. M. Rubi, and A. Pérez-Madrid, "Diffusion in tilted periodic potentials: enhancement, universality, and scaling", Phys. Rev. E **65**, 031104 (2002).

[57] B. Cichocki and K. Hinsen, "Dynamic computer simulation of concentrated hard sphere suspensions: i. simulation technique and mean square displacement data", Physica A: Statistical Mechanics and its Applications **166**, 473–491 (1990).

[58] S. Smith and R. Grima, "Fast simulation of brownian dynamics in a crowded environment", The Journal of Chemical Physics **146**, 024105 (2017).

[59] P. Kubala, M. Ciesla, and B. Dybiec, "Diffusion in crowded environments: trapped by the drift", Phys. Rev. E **104**, 044127 (2021).

[60] S. Torquato, "Unified approach to characterize microstructure", in *Random heterogeneous materials: microstructure and macroscopic properties* (Springer New York, New York, NY, 2002), pages 96–103.

[61] T. Bauer, F. Höfling, T. Munk, E. Frey, and T. Franosch, "The localization transition of the two-dimensional lorentz model", European Physical Journal ST **189**, 103–118 (2010).

[62] N. Khatri and P. S. Burada, "Confined diffusion in a random lorentz gas environment", Phys. Rev. E **102**, 012137 (2020).

[63] S. Leitmann and T. Franosch, "Time-dependent fluctuations and superdiffusivity in the driven lattice lorentz gas", Phys. Rev. Lett. **118**, 018001 (2017).

[64] A. Dechant and S.-i. Sasa, "Improving thermodynamic bounds using correlations", Phys. Rev. X **11**, 041061 (2021).

[65] L. P. Fischer, H.-M. Chun, and U. Seifert, "Free diffusion bounds the precision of currents in underdamped dynamics", Phys. Rev. E **102**, 012120 (2020).

[66] P. Pietzonka, "Classical pendulum clocks break the thermodynamic uncertainty relation", Phys. Rev. Lett. **128**, 130606 (2022).

[67] D. Levesque and L. Verlet, "Molecular dynamics and time reversibility", **72**, 519–537.